Revista Mexicana de Astronomía y Astrofísica, **59**, 11–43 (2023)

https://doi.org/10.22201/ia.01851101p.2023.59.01.02

OPTIMAL TWO-IMPULSE INTERPLANETARY TRAJECTORIES: EARTH-VENUS AND EARTH-MARS MISSIONS

L. A. Gagg Filho[1] and S. da Silva Fernandes[2]

Received March 18 2022; accepted August 23 2022

ABSTRACT

This work describes several models to design optimal interplanetary trajectories. The transfer problem consists in transferring a space vehicle from a circular low Earth orbit (LEO) to a circular low orbit around a destiny planet (Venus or Mars). Models based on the two-body, four-body, and five-body problems are considered. Also, several versions of the patched-conic approximation are utilized including a detailed version that designs a lunar swing-by maneuver. The results show that the optimal trajectories for Earth-Mars and Earth-Venus missions collide with the Moon if a lunar swing-by maneuver with an unspecified altitude of the closest approach is included in the trajectory design; however, sub-optimal trajectories that do not collide with the Moon exist, presenting a smaller fuel consumption than the trajectories without lunar swing-by and with no greater changes in the time of flight.

RESUMEN

Se describen varios modelos para diseñar trayectorias interplanetarias óptimas. El problema consiste en la transferencia de un vehículo espacial de una órbita circular baja alrededor de la Tierra (LEO) a una órbita circular baja alrededor de un planeta (Venus o Marte). Se consideran modelos basados en el problema de dos cuerpos, el de cuatro cuerpos y el de cinco cuerpos. También se utilizan versiones de la aproximación cónica parchada, incluyendo una que utiliza una maniobra de impulso lunar. Los resultados muestran que las trayectorias óptimas para misiones Tierra-Marte y Tierra-Venus colisionan con la Luna si se incluye la maniobra lunar sin especificar la distancia mínima de acercamiento. Sin embargo, existen trayectorias sub-óptimas que no colisionan con la Luna, no implican cambios en los tiempos de vuelo, y permiten un menor consumo de combustible que aquellas sin la maniobra lunar.

Key Words: Earth — interplanetary medium — Moon — space vehicles

1. INTRODUCTION

Private companies together with governmental agencies are scheduling spectacular missions to Moon. NASA, for instance, has contracts with Boeing and SpaceX to take humans to Low-Earth Orbit as part of the Commercial Crew Development program (Weinzierl 2018). This governmental agency has also envisioned the Artemis program for bringing human back to Moon (Foust 2019). The building of the Orion spacecraft with partnership of Lockheed Martin (Petrescu et al. 2017) is part of this program. The development and building of the European Service Module of Orion is a partnership with ESA and the Airbus (Meiss et al. 2016). The success of these programs, which also intend to build a space station in the cislunar space, represents a huge step to achieve a greater accomplishment: a manned mission to Mars and its future colonization. NASA and Lockheed Martin company have revealed a tight schedule of activities (Cichan et al. 2016) to establish a spacecraft in Martian orbit in order to explore Deimos and Phobos (Martian moons) and the surface of Mars (O'Dell et al. 2018). There

[1]Flight Mechanics Department, Instituto Tecnológico de Aeronáutica, Praça Marechal Eduardo Gomes 50, Vila das Acácias, 12228-900, São José dos Campos, SP, Brazil.
[2]Mathematics Department, Instituto Tecnológico de Aeronáutica, Praça Marechal Eduardo Gomes 50, Vila das Acácias, 12228-900, São José dos Campos, SP, Brazil.

are several others companies involved in commercial space activities like Blue Origin and Virgin Galactic for space tourism, Astrobotic for transportation to the Moon, Astroscale for space debris removal, Deep Space Industries for asteroid mining, and many others (Weinzierl 2018).

While manned missions are still not performed in interplanetary space, unmanned missions are exploring the Solar System for several reasons: economic (asteroid mining), colonization perspective (Mars colonization), survival purpose (the studying of dangerous asteroids that could impact Earth), and scientific purposes (life search). The Hayabusa-2 mission embraces two of these reasons: scientific and planetary defense, since it intends to return a sample of the asteroid 162173 Ryugu back to Earth and to test a kinetic impactor (Tsuda et al. 2018). In the context of asteroid missions, NASA proposes a mission to the 16 Psyche asteroid, the largest metal asteroid in the main belt (Shepard et al. 2017). Concerning life search, Europa (Jupiter's moon) is believed to be the best place in the Solar System to sustain life; in this way, NASA has proposed the Europa mission in which a space vehicle will perform several flybys around this moon in order to study it (Bayer et al. 2017). Titan, the largest moon of Saturn, is the target of a mission in which the Dragonfly, a rotorcraft lander, will explore its surface (Lorenz et al. 2018). Despite several future plans, unmanned missions are limited to the Solar System, and the manned missions are still limited to the low orbits around the Earth. A few cogitate about interstellar missions: the Breakthrough Starshot project (Daukantas 2017) intends to send a probe to reach Proxima Centauri, but several technological advances are needed.

For all these missions, trajectory determinations must be accomplished considering a mathematical model as realistic as possible. Moreover, these trajectories must be minimum-time trajectories or minimum-fuel trajectories (Prussing and Chiu 1986) or a trade-off between these two performance index as the Apollo missions. In order to perform these optimization, an initial guess is necessary, which can be a solution trajectory in a more simple model. Dei Tos and Topputo (2019), however, develop a method to optimize impulsive trajectories in a complex model that is based on a real ephemeris model. Izzo et al. (2019) utilizes machine learning based on artificial neural networks, an heuristic method, to represent the optimal guidance profile of an interplanetary mission. Abdelkhalik and Mortari (2007) utilize a genetic algorithm to solve the transfer between noncoplanar elliptical orbits utilizing impulsive maneuvers. On the other hand, Ellison et al. (2018) develop analytical methods to compute partial-derivatives of two bounded-impulsive trajectories with multiple swing-by maneuvers. Gagg Filho and da Silva Fernandes (2018) build patched-conic approximations to obtain geometrical details of interplanetary missions. Genta and Maffione (2019) state that the parameters and constraints of a trajectory are important to define the launch date, which is vital for the feasibility of the mission. Once a good initial approximation of the trajectory is obtained, a simple optimization method can be utilized as, for instance, the gradient method (Addis et al. 2011).

In the context of space missions, the present work proposes models based on the two-body, four-body, and five-body problems for trajectory determination in a preliminary mission analysis from Earth to inner planets (Venus) and outer planets (Mars) considering planar models. Among the models based on the two-body problem there are the well-known interplanetary patched-conic approximation based on the Hohmann transfer, which solves the heliocentric phase; and the interplanetary patched-conic approximation based on the Gauss problem (Bate et al. 1971), also known as Lambert's problem (Battin et al. 1978; Prussing 1979; Battin and Vaughan 1984; Gooding 1990). The characterization of the trajectory phases by the patched-conic approximations is accomplished by the definition of the sphere of influence (SOI), in a way that when the motion of the space vehicle occurs, for instance, inside the Earth's SOI, the geocentric phase is characterized.

Despite the patched-conic approximations based on the Hohmann transfer and the one based on the Gauss problem being usually used for preliminary mission analysis, these models patch the trajectory phases in an independent way. In this way, the visualization of the complete trajectory has discontinuities and information related to the complete trajectory is lost. In this sense, the present work also utilizes a patched-conic approximation based on a detailed geometry of the transfer problem (Gagg Filho and da Silva Fernandes 2018) which determines the complete trajectory by means of a two-point boundary value problem (TPBVP) and it includes a swing-by maneuver with the Moon. Broucke (1988) qualitatively mentions that the Moon is a weak gravitational accelerator; however, the present work extends the conclusion of Broucke (1988) by quantifying the saving of fuel consumption, represented by the sum of the velocity increments, when a lunar swing-by maneuver is performed in an interplan-

etary mission. The work of Faria Venditti et al. (2010) optimizes interplanetary trajectories considering swing-by maneuvers by using a patched-conic approximation in such way that no discontinuity exist for the velocity vector. Yang et al. (2019) solve a powered swing-by maneuver by using a pseudostate theory and, next, a patching technique matches the segments of the swing-by maneuver with the interplanetary trajectory in order to determine a more realistic trajectory. Lavagna et al. (2005) adopt a multi-objective strategy to minimize both fuel consumption and trip time by considering aero-gravity assist maneuvers. An evolutionary algorithm is used in this last work to avoid trapped solutions in local minima. In the present work, the patched-conic approximations with detailed geometry, and the models based on the four and five-body problem determine the complete interplanetary trajectory without any discontinuity not only in the velocity vector, but also in the position vector; moreover, the swing-by maneuver is solved together with the complete trajectory in an unique TPBVP providing an initial guess to determine the local minimum by means of a gradient technique.

In the context of the interplanetary transfer model based on the planar restricted four-body problem (PCR4BP, Sun-Earth-destiny planet-space vehicle), the present work formulates the same transfer problem with a different approach from the one described by Miele and Wang (1999b) but similar to Miele et al. (2004b), i.e, the differential equations that govern the motion of the space vehicle are written, in the present work, utilizing Cartesian coordinates (Miele and Wang 1999b utilize polar coordinates) in three distinct forms. Each form defines the differential equations for the relative motion of the space vehicle with respect to Earth, Sun, and destiny planet, respectively. The choice of the proper version of the differential equations is dependent on the predominant gravitational field acting on the space vehicle. A two-point boundary value problem (TPBVP), involving prescribed values of the initial phase angle between the space vehicle and the Earth, and the initial phase angle (rendezvous angle) of the destiny planet, is formulated. Based on this TPBVP, an one-degree of freedom optimization problem concerning the minimization of the total fuel consumption, with a prescribed rendezvous angle, is proposed. A two-degree of freedom optimization problem is also formulated, in which the rendezvous angle is taken as additional unknown. Next, the Moon's gravitational influence is included in the set of differential equations that describes the relative motion of the space vehicle to Earth; thus, the four-body problem is converted into a five-body problem in the neighborhood of Earth and a three-degree of freedom optimization problem is formulated. Therefore, this last model enables the lunar swing-by maneuver before the leaving of the space vehicle from the Earth's SOI.

The objective of this work is to analyze Earth-Mars and Earth-Venus transfers from a circular low Earth orbit (LEO) to a circular low orbit around the destiny planet (Venus or Mars) by using bi-impulsive optimal trajectories that minimize the fuel consumption in the context of the two-body, four-body, or five-body problems. This work also investigates the saving of fuel if a lunar swing-by maneuver is performed in these missions. Note that only planar problems are taken into account in the present work, which provides a good approximation for a preliminary analysis. In this case, the patched-conic approximations based on the Hohmann transfer and on the Gauss problem must already provide relevant results. The planar circular restricted four-body model is similar to the one used by Miele and Wang (1997), Miele and Wang (1999a), Miele and Wang (1999b), and by Miele et al. (2004a). In this way, the present paper extends the four-body model used by Miele by including the Moon in a planar circular restricted five-body model, and an analysis for the Earth-Venus mission is also considered.

2. MATHEMATICAL FORMULATION

This section formulates the interplanetary transfer based on the two-body problem, the restricted four-body problem, and the restricted five-body problem. The interplanetary mission consists in transferring a space vehicle from a low Earth orbit (LEO) to a low Mars orbit - LM_tO(or, to a low Venus orbit - LVO) by applying two impulses tangential to the terminal orbits. The first velocity increment Δv_{LEO} inserts the space vehicle into a transfer trajectory, and the second velocity increment Δv_{LM_tO} (or, Δv_{LVO}) brakes the vehicle circularizing its motion at the LM_tO (or, LVO). The fuel consumption is represented by the total characteristic velocity $\Delta v_{Total} = \Delta v_{LEO} + \Delta v_{LM_tO}$ (or, $\Delta v_{LEO} + \Delta v_{LVO}$) (Marec 1979). The terminal orbits, the planet orbits and the Moon orbit are considered circular and coplanar, in a way that the motion of the space vehicle occurs in the plane of these orbits. Table 1 shows the approximate eccentricity and inclination of the celestial body orbits.

Note in Table 1 that the inclinations of the celestial body orbits used in the present paper are small (the largest is that of the Moon and it is equal to

TABLE 1

INCLINATION AND ECCENTRICITY OF THE MAIN BODY ORBITS (JPL/NASA)

	Eccentricity	Inclination to the mean ecliptic
Venus	0.0067	3.3977°
Earth-Moon barycenter	0.0167	0.0005°
Moon	0.0554	5.1600°
Mars	0.0933	1.8518°

5.6°), so the orbital motion of the Moon, Earth, Mars, Venus and space vehicle is simplified on the ecliptic plane. In the same way, the orbits of the celestial bodies are considered circular as their eccentricities are small (the largest is that of Mars and it is equal to 0.0933).

Among the models based on the two-body problem there are: the classic patched-conic approximation based on the Hohmann transfer, the patched-conic approximation based on the Gauss problem, the patched-conic approximation with detailed geometry, and the patched-conic approximation with a lunar swing-by maneuver. For all the models based on patched-conic approximations, the interplanetary trajectory is divided in phases, which are defined by the sphere of influence (SOI) of the main bodies. In this way, the patched-conic approximations have, at least, three phases: the geocentric phase, where only the gravitational field of the Earth is considered; the heliocentric phase, where only the gravitational field of the Sun is considered; and, the planetocentric phase, where only the gravitation field of the destiny planet is considered. These models are briefly discussed below. In order to simplify the notation, Mars is considered to be the destiny planet without loss of generality.

2.1. *Patched-Conic Approximation Based on the Hohmann Transfer*

For the patched-conic approximation based on the Hohmann transfer, the heliocentric phase is solved first (Bate et al. 1971). For this phase, the Hohmann transfer (Bate et al. 1971; Prussing and Conway 1993) is utilized to estimate the parameters of the elliptic transfer trajectory that defines the heliocentric phase, which includes the Hohmann velocity increments $\Delta v_{0,Hohmann}$ and $\Delta v_{f,Hohmann}$. Next, the geocentric and the planetocentric trajectories are simultaneously determined by considering them as hyperbolic, with their excess velocities, $\Delta v_{\infty,geo}$ and $\Delta v_{\infty,pla}$, equal to the Hohmann velocity increments, $\Delta v_{0,Hohmann}$ and $\Delta v_{f,Hohmann}$ respectively. By using well-known results of the two-body problem, it is now possible to determine the initial velocity, v_0, of the space vehicle right after the application of Δv_{LEO}, and the final velocity, v_f, of the space vehicle right before the application of Δv_{LM_tO} (or Δv_{LVO}). The velocity increments are calculated as:

$$\Delta v_{LEO} = v_0 - \sqrt{\frac{\mu_E}{r_0}}, \tag{1}$$

$$\Delta v_{LM_tO} = v_f - \sqrt{\frac{\mu_{M_t}}{r_f}}, \tag{2}$$

where μ_E and μ_{M_t} are the Earth and Mars gravitational parameters, respectively; r_0 is the radius of the circular LEO, and, r_f is the radius of the circular LM_tO.

2.2. *Patched-Conic Approximation Based on the Gauss Problem*

According to the Hohmann transfer in the previous section, the space vehicle describes an elliptic heliocentric trajectory making a 180° arc in true anomaly (the transfer ellipse is tangent simultaneously to the terminal orbits). However, if it is desired to reach the SOI of Mars with a smaller travel time, a smaller arc of true anomaly must be prescribed. In this way, the vectors of the excess velocities must be obtained by another procedure. To achieve this goal, the heliocentric phase is solved with the Gauss problem (also known as Lambert problem [1]) (Bate et al. 1971; Battin et al. 1978; Prussing 1979; Battin and Vaughan 1984; Gooding 1990). To apply the Gauss problem, the magnitude of two position vectors of the space vehicle must be provided, as well as the time of flight and the true anomaly variation Δf between these two vectors and the direction of motion. Since the elliptic trajectory is defined from the boundary of the Earth's SOI to the boundary of Mars' SOI, the magnitudes of these two vectors are the Earth-Sun distance, D_E, and the Mars-Sun distance, D_{M_t}. Once the excess velocities, $\Delta v_{0,Gauss}$ and $\Delta v_{f,Gauss}$, are obtained based on the Gauss problem, the initial velocity v_0 and the final velocity

[1] In the classic Lambert problem, the two position vectors (or equivalently the magnitude of the position vectors and the variation of the true anomaly) are provided together with the time of flight. Then, the velocity vectors are calculated without any optimization. However, if the variation of the true anomaly or the time of flight is not prescribed, that is, it is taken as unknown, then one can formulate an one-degree optimization problem (Problem 1 and Problem 2).

v_f of the space vehicle are calculated; and the velocity increments, Δv_{LEO} and Δv_{LM_tO}, applied to the space vehicle, are determined using equations (1) and (2), respectively.

Note that the Gauss problem is solved for a prescribed value of time of flight; therefore, an optimization problem is enunciated below by setting the time of flight as an unknown to be determined in order to obtain the solution with minimum Gauss velocity increment $\Delta v_{Total,Gauss}$.

Problem 1 *"Given the value of Δf, the direction of motion, and prescribing the magnitudes of two position vectors (D_E and D_{M_t}, for instance), determine the time of flight Δt between these two vectors that minimizes the function*

$$F(\Delta t): \quad \Delta v_{Total,Gauss} = \Delta v_{0,Gauss} + \Delta v_{f,Gauss}." \tag{3}$$

An equivalent optimization problem can be also enunciated with a prescribed time of flight by setting the true anomaly variation Δf as unknown to minimize the fuel consumption. This second optimization problem is enunciated below.

Problem 2 *"Given the value of time of flight, the direction of motion, and prescribing the magnitudes of two position vectors (D_E and D_{M_t}, for instance), determine the true anomaly Δf between these two vectors that minimizes the function*

$$F(\Delta f): \quad \Delta v_{Total,Gauss} = \Delta v_{0,Gauss} + \Delta v_{f,Gauss}." \tag{4}$$

2.3. *Patched-Conic Approximation with Detailed Geometry*

In the patched-conic approximation based on the Hohmann transfer and the one based on the Gauss problem, the heliocentric phase is first solved to determine the excess velocities. For these models, it is not possible to build the complete Earth-Mars trajectory without discontinuity between the points that connect the phases. This section shortly comments about a new patched-conic approximation in which the excess velocities are determined through a detailed geometry; it is based on an extension of the lunar patched-conic approximation, as described by Arthur Gagg Filho and da Silva Fernandes (2016). For this model, the geocentric phase is solved first, followed by the heliocentric phase, and finally, the planetocentric is determined. The inertial reference frame S_{XY} is taken with the Sun at origin, the X-axis

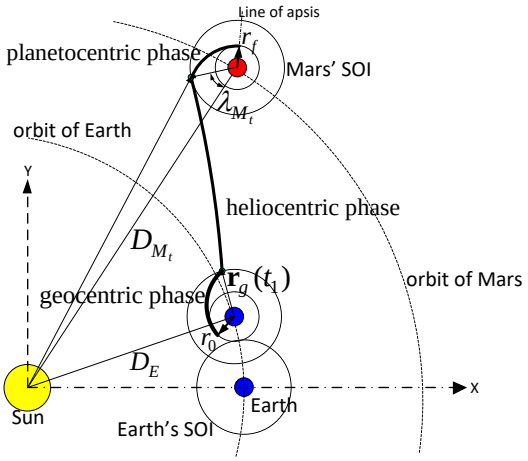

Fig. 1. Geometry of the patched-conic approximation. The color figure can be viewed online.

pointing towards Earth at the initial time, and with the Y-axis orthogonal to the X-axis according to Figure 1. Therefore, when the complete trajectory, Figure 1, is determined, one must compare the calculated arrival condition of the space vehicle with the prescribed arrival condition. In this way, the complete trajectory is obtained by solving a two-point boundary value problem (TPBVP) as enunciated below

Problem 3 *"Given the terminal altitudes h_{LEO} and h_{LM_tO}, and prescribing the initial phase angle $\theta_{EP}(0)$ of the space vehicle with the Earth and the phase angle λ_{Mt}, which describes the arrival geometry at the Mars' SOI, determine the initial velocity v_0 subjected to the final constraint:*

$$g(v_0): \quad r_{p_{pla}} - r_f = 0, \tag{5}$$

where $r_{p_{pla}}$ is the calculated pericenter distance of the planetocentric phase, and r_f is the prescribed radius of the LM_tO."

The velocity increments, Δv_{LEO} and Δv_{LM_tO}, applied to space vehicle are determined using equations (1) and (2), respectively. Note that an optimization problem can be enunciated in order to determine the value of λ_{Mt} that minimizes the fuel consumption Δv_{Total}.

2.4. *Patched-Conic Approximation with a Lunar Swing-by Maneuver*

This patched-conic model is similar to the patched-conic approximation presented in § 2.3, but with two more phases in order to include a lunar

swing-by maneuver, and with the inertial reference frame S_{XY} centered on the Sun with the X-axis parallel to the Earth-Moon line at the initial time (see Figure 2). In this way, the complete trajectory is described by five phases: a first elliptic geocentric phase is characterized from the departure of the space vehicle from the LEO until it reaches the boundary of the Moon's SOI; next, an hyperbolic selenocentric phase models the lunar swing-by maneuver; a second, but hyperbolic geocentric phase is defined from the departure from the Moon's SOI until the reaching of the boundary of the Earth's SOI; next, an elliptic heliocentric phase is defined from the departure of the Earth's SOI until the space vehicle reaches the Mars' SOI; finally, the hyperbolic planetocentric phase is characterized from the boundary of the Mars' SOI until the arrival at the LM_tO. The complete formulation of this patched-conic approximation can be found in Gagg Filho and da Silva Fernandes (2018). Since there is a lunar swing-by maneuver in this model, an intermediary constraint is included. This constraint defines the pericenter altitude of the selenocentrinc phase. Therefore, the TPBVP can be enunciated as it follows:

Problem 4 *"Given the terminal altitudes h_{LEO} and h_{LM_tO}, and prescribing the phase angle λ_1, which describes the arrival geometry at the Moon's SOI, and the phase angle λ_{Mt}, which describes the arrival geometry at the Mars' SOI, determine the initial velocity v_0 and the phase angles λ_S, which describes the departure geometry from the Earth's SOI, subjected to the final constraint:*

$$g(\lambda_S): \quad r_{p_{pla}} - r_f = 0, \tag{6}$$

and subject to the intermediary constraint:

$$g_0(v_0): \quad r_{pM} - r_{sP} = 0, \tag{7}$$

where r_{sP} is the prescribed distance of close encounter with the Moon, and r_{pM} is the calculated pericenter distance of the selenocentric phase."

The velocity increments, Δv_{LEO} and Δv_{LM_tO}, applied to the space vehicle are determined using equations (1) and (2), respectively. Note that an optimization problem with two-degree of freedom can be enunciated in order to determine the values of λ_{Mt} and λ_1 which minimize the fuel consumption Δv_{Total}.

2.5. *Interplanetary Transfer Problem Based on the Four-Body Problem*

In this section, the interplanetary transfer problem based on the planar circular restricted four-body problem (PCR4BP), in which the three primaries are the Earth, the Sun and Mars, and the fourth body is the space vehicle, is formulated. A mathematical development can be found in Miele and Wang (1999b), which utilizes polar coordinates to formulate the problem; however, the present work formulates the differential equations in Cartesian coordinates similar to Miele et al. (2004b). To solve the interplanetary transfer problem, consider an inertial reference frame S_{XY} centered on the Sun with the X-axis pointing to Earth at the initial time t_0, and with the Y-axis orthogonal to the X-axis at the direction of orbital motion of the Earth around the Sun (Figure 3). Despite the space vehicle being subjected to

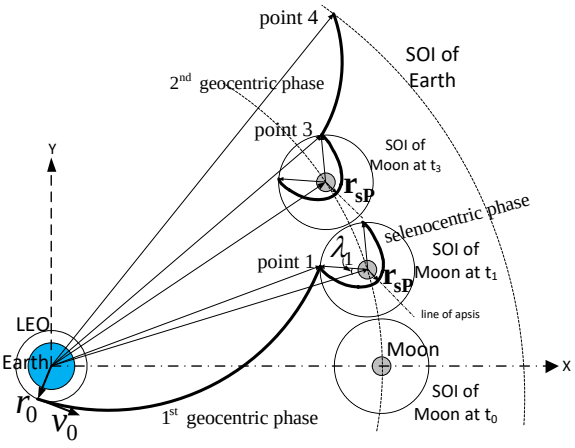

(a) Geocentric and selenocentric phases.

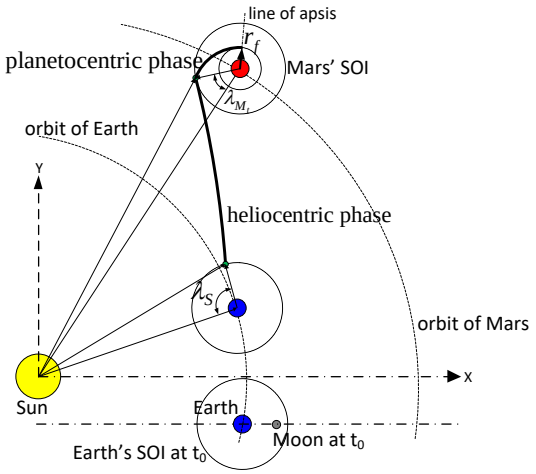

(b) Heliocentric and planetocentric phases.

Fig. 2. Patched-conic approximation with swing-by. Modified from Gagg Filho and da Silva Fernandes (2018). The color figure can be viewed online.

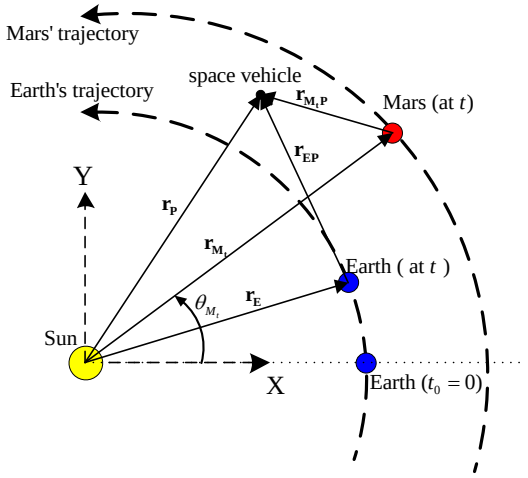

Fig. 3. Inertial reference frame S_{XY} for the PCR4BP. The color figure can be viewed online.

the gravitational fields of the three primaries during the whole trajectory, three phases of the trajectories are considered to formulate the problem: the geocentric phase, the heliocentric phase, and the planetocentric phase. This procedure provides a better accuracy in the numerical integration of the differential equations because a suitable normalization is used in each phase. For example, when the space vehicle is in the neighborhood of Earth, the gravitational field of this body is predominant; thus, the system of differential equations is written based on the relative motion of the space vehicle with respect to Earth. In this case, the normalization is performed by utilizing the Earth's parameters. On the other hand, when the space vehicle is far from Earth and Mars, the gravitational field of the Sun is predominant; therefore, the system of differential equations is written based on the relative motion of the space vehicle with respect to Sun. The same explanation follows when the space vehicle is in the neighborhood of Mars. In order to characterize the different phases, the concept of SOI is utilized. In this model, the concept of SOI is only applied to separate the phases; thus, the space vehicle is still subjected to the gravitational fields of the primaries along the whole trajectory.

2.5.1. *Geocentric Phase*

At the initial time, the space vehicle is at the *LEO*. After applying the first velocity increment Δv_{LEO}, the space vehicle is inserted into an interplanetary transfer trajectory. So, at the beginning of the mission, the space vehicle is in the neighborhood of the Earth and its motion is described by the following system of differential equations:

$$\ddot{x}_{EP} = -\frac{\mu_S}{r_P^3}(x_{EP}+x_E) - \frac{\mu_E}{r_{EP}^3}(x_{EP}) - \frac{\mu_{M_t}}{r_{M_tP}^3}(x_{EP}+x_E-x_{M_t}) + \frac{\mu_S}{r_E^3}(x_E), \tag{8}$$

$$\ddot{y}_{EP} = -\frac{\mu_S}{r_P^3}(y_{EP}+y_E) - \frac{\mu_E}{r_{EP}^3}(y_{EP}) - \frac{\mu_{M_t}}{r_{M_tP}^3}(y_{EP}+y_E-y_{M_t}) + \frac{\mu_S}{r_E^3}(y_E), \tag{9}$$

where (x_{EP}, y_{EP}) are the components of the position vector of the space vehicle with respect to Earth; r_P, r_{EP}, and, r_{M_tP} are the magnitude of the position vector of the space vehicle with respect to, respectively, Sun, Earth, and the destiny planet (Mars); and μ_S is the gravitational parameter of the Sun. (x_E, y_E) and (x_{M_t}, y_{M_t}) define the components of the position vectors of the Earth and Mars, respectively, and are calculated as follows:

$$x_E = D_E\cos(\omega_E t), \tag{10}$$

$$y_E = D_E\sin(\omega_E t), \tag{11}$$

$$x_{M_t} = D_{M_t}\cos[\omega_{M_t}t + \theta_{M_t}(0)], \tag{12}$$

$$y_{M_t} = D_{M_t}\sin[\omega_{M_t}t + \theta_{M_t}(0)], \tag{13}$$

where ω_E and ω_{M_t} are the angular velocities (mean motions) of Earth and Mars, respectively, around Sun (see Table 2); D_E and D_{M_t} are, respectively, the Sun-Earth distance and the Sun-Mars distance; $\theta_{M_t}(0)$ is the initial phase angle, also called the rendezvous angle, of Mars in the S_{XY} reference frame.

The time derivative expressions of equations 10 – 13 provide the velocity vector components:

$$\dot{x}_E(t) = -\omega_E D_E\sin(\omega_E t), \tag{14}$$

$$\dot{y}_E(t) = \omega_E D_E\cos(\omega_E t), \tag{15}$$

$$\dot{x}_{M_t}(t) = -\omega_{M_t} D_{M_t}\sin[\omega_{M_t}t + \theta_{M_t}(0)], \tag{16}$$

$$\dot{y}_{M_t}(t) = \omega_{M_t} D_{M_t}\cos[\omega_{M_t}t + \theta_{M_t}(0)]. \tag{17}$$

Initial Conditions

The initial conditions that define the beginning of integration of the differential equation system (equations 8 and 9), are given by the components of the position and velocity vectors of the space vehicle with respect to Earth at t_0, i.e, at the time right after the application of Δv_{LEO}:

$$x_{EP}(0) = r_{EP}(0)\cos\left[\theta_{EP}(0)\right], \tag{18}$$

TABLE 2

PLANETARY DATA

Planet	Distance to the Sun (km)	Radial Distance (km)	gravitational parameter μ (km^3/s^2)	mean motion (rad/s)	SOI radius (km)
Venus[1]	1.0815×10^8	6051.8	32.4776×10^4	$3.23861161 \times 10^{-7}$	615976.52
Earth[2]	1.4960×10^8	6378.2	39.8600×10^4	$1.99177621 \times 10^{-7}$	923502.24
Mars[2]	2.2790×10^8	3397.0	4.2830×10^4	$1.05850987 \times 10^{-7}$	577723.87

[1]Calculated distance from the data of JPL/NASA.

[2]Calculated distance from the data found in Miele and Wang (1999b).

$$y_{EP}(0) = r_{EP}(0)\sin\left[\theta_{EP}(0)\right], \tag{19}$$

$$\dot{x}_{EP}(0) = -\left[\sqrt{\frac{\mu_E}{r_{EP}(0)}} + \Delta v_{LEO}\right]\sin\left[\theta_{EP}(0)\right], \tag{20}$$

$$\dot{y}_{EP}(0) = \left[\sqrt{\frac{\mu_E}{r_{EP}(0)}} + \Delta v_{LEO}\right]\cos\left[\theta_{EP}(0)\right], \tag{21}$$

where $r_{EP}(0) = r_{EP_0}$ is the Earth-space vehicle distance at t_0 given by $R_E + h_{LEO}$ with R_E denoting the mean equatorial radius of Earth and h_{LEO} denoting the altitude of the LEO; and, $\theta_{EP}(0)$ is the initial phase angle of the space vehicle with respect to Earth in the S_{XY} reference frame. The LEO is assumed in the counterclockwise direction (direct orbit).

The numerical integration of equations 8 and 9 is performed from $t = t_0$ to $t = t_1$, at which the following constraint becomes true:

$$g_{0_{GEO}} : r_{EP}(t_1) > R_{ST}, \tag{22}$$

where R_{ST} is the radius of the SOI of the Earth. The heliocentric phase initiates when the constraint $g_{0_{GEO}}$ is satisfied.

2.5.2. *Heliocentric Phase*

In this phase, the gravitational field of the Sun is predominant and it initiates when the space vehicle leaves the Earth's SOI. In this way, the system of differential equations that describes the motion of the space vehicle is written with its position and velocity vectors with respect to the inertial frame as following:

$$\ddot{x}_P = -\frac{\mu_S}{r_P^3}(x_P) - \frac{\mu_E}{r_{EP}^3}(x_P - x_E) - \frac{\mu_{M_t}}{r_{M_tP}^3}(x_P - x_{M_t}), \tag{23}$$

$$\ddot{y}_P = -\frac{\mu_S}{r_P^3}(y_P) - \frac{\mu_E}{r_{EP}^3}(y_P - y_E) - \frac{\mu_{M_t}}{r_{M_tP}^3}(y_P - y_{M_t}), \tag{24}$$

where (x_P, y_P) are the components of the position vector of the space vehicle with respect to Sun (origin of the inertial reference system).

Initial Conditions

The initial conditions of the system defined by equations (23) and (24) are the components of the position and velocity vectors of the space vehicle with respect to Sun at time t_1. In this way, one has

$$x_P(t_1) = x_E(t_1) + x_{EP}(t_1), \tag{25}$$

$$y_P(t_1) = y_E(t_1) + y_{EP}(t_1), \tag{26}$$

$$\dot{x}_P(t_1) = \dot{x}_E(t_1) + \dot{x}_{EP}(t_1), \tag{27}$$

$$\dot{y}_P(t_1) = \dot{y}_E(t_1) + \dot{y}_{EP}(t_1). \tag{28}$$

For the calculation of these initial conditions it is enough to determine the components of the position and velocity vectors of the Earth at t_1 by utilizing equations 10, 11, 14 and 15; and to utilize the components of position and velocity vectors of the space vehicle with respect to Earth at t_1, which are provided as the state variables by the end of the integration of the geocentric phase. Once the initial conditions are established, the differential equation system, equations 23 and 24, is integrated from $t = t_1$ to $t = t_2$, when the space vehicle reaches the boundary of the SOI of Mars (or Venus) defined by the following constraint:

$$g_{0_{HELIO}} : r_{M_tP}(t_2) < R_{SM_t}, \tag{29}$$

where R_{SM_t} is the radius of the SOI of Mars. The planetocentric phase initiates when the constraint $g_{0_{HELIO}}$ is satisfied.

2.5.3. *Planetocentric Phase*

The planetocentric phase initiates when the space vehicle reaches the boundary of Mars' SOI; thus, the gravitational field of Mars becomes predominant.

The system of differential equations is expressed with the components of the position and velocity vectors of the space vehicle with respect to Mars as below:

$$\ddot{x}_{M_tP} = -\frac{\mu_S}{r_P^3}(x_{M_tP}+x_{M_t}) - \frac{\mu_E}{r_{EP}^3}(x_{M_tP}+x_{M_t}-x_E) - \frac{\mu_{M_t}}{r_{M_tP}^3}(x_{M_tP}) + \frac{\mu_S}{r_{M_t}^3}(x_{M_t}), \tag{30}$$

$$\ddot{y}_{M_tP} = -\frac{\mu_S}{r_P^3}(y_{M_tP}+y_{M_t}) - \frac{\mu_E}{r_{EP}^3}(y_{M_tP}+y_{M_t}-y_E) - \frac{\mu_{M_t}}{r_{M_tP}^3}(y_{M_tP}) + \frac{\mu_S}{r_{M_t}^3}(y_{M_t}), \tag{31}$$

where (x_{M_tP}, y_{M_tP}) are the components of the position vector of the space vehicle with respect to Mars.

Initial Conditions

The initial conditions of the system defined by equations (30) and (31) are the components of the position and velocity vectors of the space vehicle to Mars at time t_2. These components are expressed by:

$$x_{M_tP}(t_2) = x_P(t_2) - x_{M_t}(t_2), \tag{32}$$

$$y_{M_tP}(t_2) = y_P(t_2) - y_{M_tP}(t_2), \tag{33}$$

$$\dot{x}_{M_tP}(t_2) = \dot{x}_P(t_2) - \dot{x}_{M_tP}(t_2), \tag{34}$$

$$\dot{y}_{M_tP}(t_2) = \dot{y}_P(t_2) - \dot{y}_{m_tP}(t_2). \tag{35}$$

For the calculation of these initial conditions it is enough to determine the components of the position and velocity vectors of Mars at t_2 by utilizing equations 12, 13, 16 and 17; and to utilize the components of position and velocity vectors of the space vehicle with respect to Sun at t_2, which are provided as the state variables by the end of the integration of the heliocentric phase. Once the initial conditions are established, the differential equation system, equations (30) and (31), is integrated from $t = t_2$ to $t = T$, the moment right before the application of the second velocity increment that circularizes the space vehicle in the low orbit of the destiny planet according to the final constraints. Note that, in order to switch between the phases, the position vector of the primaries must be monitored.

2.5.4. *Two-Point Boundary Value Problem*

According to § 2.5.1 and § 2.5.3, one can determine the trajectory by integrating the system of differential equations of each phase if the initial conditions of equations (8) and (9) are given. However, the final conditions must agree with the terminal constraints at the LM_tO. Therefore, a TPBVP is enunciated as it follows:

Problem 5 *"Given the terminal altitudes h_{LEO} and h_{LM_tO}, and prescribing the initial phase angle $\theta_{EP}(0)$ of the space vehicle with respect to Earth and the initial phase angle of Mars $\theta_{M_t}(0)$, determine the set of variables $(\Delta v_{LEO}, \Delta v_{LM_tO}, T)$ subject to the final constraints:*

$$g_1: \quad (x_{M_tP}(T))^2 + (y_{M_tP}(T))^2 - (r_{M_tP}(T))^2 = 0, \tag{36}$$

$$g_2: \quad (\dot{x}_{M_tP}(T))^2 + (\dot{y}_{M_tP}(T))^2 - \left[\sqrt{\frac{\mu_{M_t}}{r_{M_tP}(T)}} + \Delta v_{LM_tO}\right]^2 = 0, \tag{37}$$

$$g_3: \quad (x_{M_tP}(T))(\dot{y}_{M_tP}(T)) - (y_{M_tP}(T))(\dot{x}_{M_tP}(T)) \pm r_{M_tP}(T)\left[\sqrt{\frac{\mu_{M_t}}{r_{M_tP}(T)}} + \Delta v_{LM_tO}\right] = 0, \text{"} \tag{38}$$

where the upper (lower) sign in equation (38) indicates a clockwise (counterclockwise) arrival at the $LMtO$. This problem is solved by means of the Newton-Raphson algorithm.

Note also that the angles $\theta_{EP}(0)$ and $\theta_{M_t}(0)$ are prescribed. By taking advantage of this fact, two optimization problems are next enunciated.

2.5.5. *One-Degree of Freedom Optimization Problem*

If there is a solution of the TPBVP for each value of $\theta_{EP}(0)$ with $\theta_{M_t}(0)$ prescribed; then there must exist an optimal value of $\theta_{EP}(0)$ that minimizes the fuel consumption. Therefore, the following one-degree of freedom optimization problem is enunciated:

Problem 6 *"Given the terminal altitudes h_{LEO} and h_{LM_tO}, and prescribing $\theta_{M_t}(0)$, determine the set of variables (Δv_{LEO}, Δv_{LM_tO}, T, $\theta_{EP}(0)$) that minimizes the function*

$$F: \quad \Delta v_{Total} = \Delta v_{LEO} + \Delta v_{LM_tO}, \tag{39}$$

subject to the final constraints g_1, g_2 and g_3 defined by equations (36), (37) and (38), respectively. "

2.5.6. *Two-Degree of Freedom Optimization Problem*

According to Problem 5, the phase angles $\theta_{EP}(0)$ and $\theta_{M_t}(0)$ must be prescribed in order to solve the TPBVP. However, one can take both angles as unknowns to solve a two-degree optimization problem as enunciated below:

Problem 7 *"Given the terminal altitudes h_{LEO} and h_{LM_tO}, determine the set of variables (Δv_{LEO}, Δv_{LM_tO}, T, $\theta_{EP}(0)$, $\theta_{M_t}(0)$) that minimizes the function*

$$F: \quad \Delta v_{Total} = \Delta v_{LEO} + \Delta v_{LM_tO}, \tag{40}$$

subject to the final constraints g_1, g_2 and g_3 defined by equations (36), (37) and (38), respectively."

2.6. *Interplanetary Transfer Problem Based on the Five-Body Problem*

This model extends the formulation of the interplanetary transfer based on the PCR4BP (§ 2.5) by including a lunar swing-by maneuver. In this sense the system of differential equations of the geocentric phase, equations (8) and (9), is modified by adding the gravitational attraction of the Moon, converting the PCR4BP into a planar circular restricted five-body problem (PCR5BP). Thus, the new system of differential equations that describes the motion of the space vehicle at the neighborhood of Earth is described as below:

$$\ddot{x}_{EP} = -\frac{\mu_S}{r_P^3}(x_{EP}+x_E) - \frac{\mu_E}{r_{EP}^3}(x_{EP}) - \frac{\mu_{M_t}}{r_{M_tP}^3}(x_{EP}+x_E-x_{M_t}) - \frac{\mu_M}{r_{PM}^3}(x_{EP}-x_{ME}) + \frac{\mu_S}{r_E^3}(x_E), \tag{41}$$

$$\ddot{y}_{EP} = -\frac{\mu_S}{r_P^3}(y_{EP}+y_E) - \frac{\mu_E}{r_{EP}^3}(y_{EP}) - \frac{\mu_{M_t}}{r_{M_tP}^3}(y_{EP}+y_E-y_{M_t}) - \frac{\mu_M}{r_{PM}^3}(y_{EP}-y_{ME}) + \frac{\mu_S}{r_E^3}(y_E), \tag{42}$$

where r_{PM} is the magnitude of the position vector of the space vehicle with respect to Moon, and, (x_{ME}, y_{ME}) are the components of the position vector of the Moon with respect to Earth determined as it follows

$$x_{ME} = D_M \cos(\theta_M(0) + \omega_M t), \tag{43}$$

$$y_{ME} = D_M \sin(\theta_M(0) + \omega_M t). \tag{44}$$

The Earth-Moon mean distance is denoted by D_M in equations 43 and 44, ω_M is the angular velocity (mean motion) of the Moon around the Earth, and $\theta_M(0)$ is the initial phase angle of the Moon with respect to the X-axis of the inertial reference frame S_{XY}.

When the space vehicle leaves the Earth's SOI, the system of differential equation must be rewritten with the position vector of the space vehicle with respect to Sun in a similar way to equations (41) and (42). In the same way, when the space vehicle enters the SOI of the destiny planet, another system of differential equations is used with the position vector of the space vehicle with respect to the destiny planet. To simplify numerical computation, the gravitational field of the Moon is neglected in the heliocentric and planetocentric phases. If the initial condition for the integration of the equations of motion (equations 41 and 42) is accurate enough, the lunar swing-by maneuver will occur naturally; therefore, there is no intermediary constraint that defines the swing-by maneuver.

2.6.1. *The Two-Point Boundary Value Problem (TPBVP)*

The TPBVP of this interplanetary transfer problem is similar to the one based on the four-body problem, but with an additional parameter: the initial phase angle of the Moon $\theta_M(0)$ with respect to the X-axis of the inertial reference frame S_{XY}. Therefore, the TPBVP is enunciated as:

Problem 8 *"Given the terminal altitudes h_{LEO} and h_{LM_tO}, and, prescribing the phase angles $\theta_{EP}(0)$, $\theta_{M_t}(0)$, and $\theta_M(0)$, determine the set of variables (Δv_{LEO}, Δv_{LM_tO}, T), subject to the final constraints g_1, g_2 and g_3 defined by equations (36), (37) and (38), respectively."*

Note that an optimization problem of two-degree of freedom is also formulated as Problem 7 but with $\theta_M(0)$ as a prescribed parameter. Moreover, one can prescribe two of the three angles [$\theta_{EP}(0)$, $\theta_{M_t}(0)$, and $\theta_M(0)$] to solve an one-degree optimization problem; or, one can set $\theta_M(0)$ as also an unknown to be determined in a three-degree optimization problem enunciated as:

Problem 9 *"Given the terminal altitudes h_{LEO} and h_{LM_tO}, determine the set of variables $(\Delta v_{LEO}, \Delta v_{LM_tO}, T, \theta_{EP}(0), \theta_{M_t}(0), \theta_M(0))$, that minimizes the function*

$$F: \quad \Delta v_{Total} = \Delta v_{LEO} + \Delta v_{LM_tO}, \tag{45}$$

subject to the final constraints g_1, g_2 and g_3 defined by equations (36), (37) and (38), respectively."

3. RESULTS

This section is divided in two topics. The first one presents results about interplanetary missions without a lunar swing-by maneuver. The second one presents interplanetary missions with an intermediary lunar swing-by maneuver. In the first part, a study is performed by solving TPBVPs by using the interplanetary patched-conic approximations and the model based on the PCR4BP. Next, the one and the two-degree of freedom optimization problems are solved in the context of the PCR4BP to determine the optimal trajectories. Penalties on the fuel consumption are quantified if the space vehicle does not depart specifically from the optimal geometry. In the second part, the trajectories determined by the patched-conic approximation are utilized as an initial guesses to solve the TPBVP (Problem 8) based on the PCR5BP. By using this last solution, the three-degree optimization problem is solved to determine the optimal interplanetary trajectories with a lunar swing-by maneuver in the context of the PCR5BP.

All the TPBVPs are solved by means of a Newton-Raphson algorithm (Press et al. 1997), and the optimization problems are solved by means of the Sequential Gradient Restoration Algorithm (Miele et al. 1969). The computational codes are implemented using FORTRAN 90.

3.1. *Interplanetary Missions Without Swing-by Maneuver*

This section studies interplanetary missions without a lunar swing-by maneuver. For this study, the patched-conic with detailed geometry, § 2.3, and the problem based on the four-body problem, § 2.5, are used. An inner transfer, Earth-Venus, and an outer transfer, Earth-Mars, are utilized to exemplify the results. The terminal altitudes are: $h_{LEO} = 463\,\text{km}$, $h_{M_tO} = 200\,\text{km}$ for Mars mission and $h_{LVO} = 200\,\text{km}$ for Venus mission. The eccentricities of the main body orbits are neglected as already discussed. The Earth-Moon mean distance is $D_M = 384400\,\text{km}$, the SOI radius of the Moon is 66300 km, and the mean motion of the Moon's orbit around Earth is $\omega_M = 2.6653 \times 10^{-6}\,\text{rad/s}$. The gravitational parameter of the Sun is $\mu_S = 1.327 \times 10^{11}$ (Miele and Wang 1999b). The data for Earth, Venus and Mars are presented in Table 2.

3.1.1. *Interplanetary Patched-Conic Approximations*

According to Problem 3, the TPBVP is solved by setting two parameters: $\theta_{EP}(0)$ and λ_{Mt} (or, λ_V for the Venus mission). However, solutions may not exist for some values of these parameters. With this in mind, the patched-conic approximation based on Hohmann transfer (§ 2.1) and the patched-conic approximation based on the Gauss problem (§ 2.2) help to glimpse solutions for Problem 3 providing values for $\theta_{EP}(0)$. Figures 4 and 5 plot the solutions of the main parameters: Δv_{LEO}, Δv_{LM_tO}, Δv_{Total}, T and $\theta_{M_t}(T)$ for Mars mission or $\theta_V(T)$ for the Venus mission against $\theta_{EP}(0)$ and λ_{Mt}. These figures are the solution of several TPBVPs, in which different sets of $\theta_{EP}(0)$ and λ_{Mt} are used. In this way, for each value of $\theta_{EP}(0)$, solutions are searched for λ_{Mt} within the interval $[0°, 180°]$ with a $1°$ step; and, solutions for λ_V within the interval $[0°, -180°]$ with a $-1°$ step. Observe that, according to the Hohmann transfer, the solutions for the Earth-Mars mission are to be found with an arrival ahead the SOI of Mars $\lambda_{Mt} \in [0°, 180°]$, and the solutions for the Earth-Venus mission are to be found with an arrival behind the SOI of Venus, $\lambda_V \in [-180°, 0°]$. For the parametrization of $\theta_{EP}(0)$, the interval is indirectly specified by the Gauss problem: for the Earth-Mars mission the time of flight in the Gauss problem is specified within the interval $[215, 265]$ days with a 1 day step. Then, the Gauss problem is solved by prescribing the time of flight and using the true anomaly as an unknown to minimize the fuel consumption (Problem 2). Therefore, there is a relation between the time of flight and $\theta_{EP}(0)$ given by the Gauss problem. The same procedure is performed for the Earth-Venus transfer in which the time of flight is specified within the interval $[70, 180]$ days. In order to illustrate only the practical results, Figures 4 and 5 show only results in which Δv_{Total} does not exceed 10 km/s. Both clockwise and counterclockwise arrivals are considered.

The model based on the interplanetary patched-conic approximation with detailed geometry also sets the motion direction at the final terminal orbit (LM_tO or LVO) which can be clockwise or counterclockwise. In terms of fuel consumption, the motion direction almost does not change the velocity increments for the Earth-Mars mission (Figures 4a–4c). In fact, the results of both direction are overlapping each other in these figures. The same occurs for the Earth-Venus mission (Figures 5a–5c). Moreover, the phase angles $\theta_{M_t}(T)$ and $\theta_V(T)$ (Figures 4e and 5e) and the time of flight (Figures 4d and 5d) do not change with respect to the arrival direction. For the Earth-Mars mission, the best set $(\theta_{EP}(0), \lambda_{Mt})$ for small fuel consumption impacts mainly on the reduction of Δv_{LM_tO}: while Δv_{LEO} can decrease

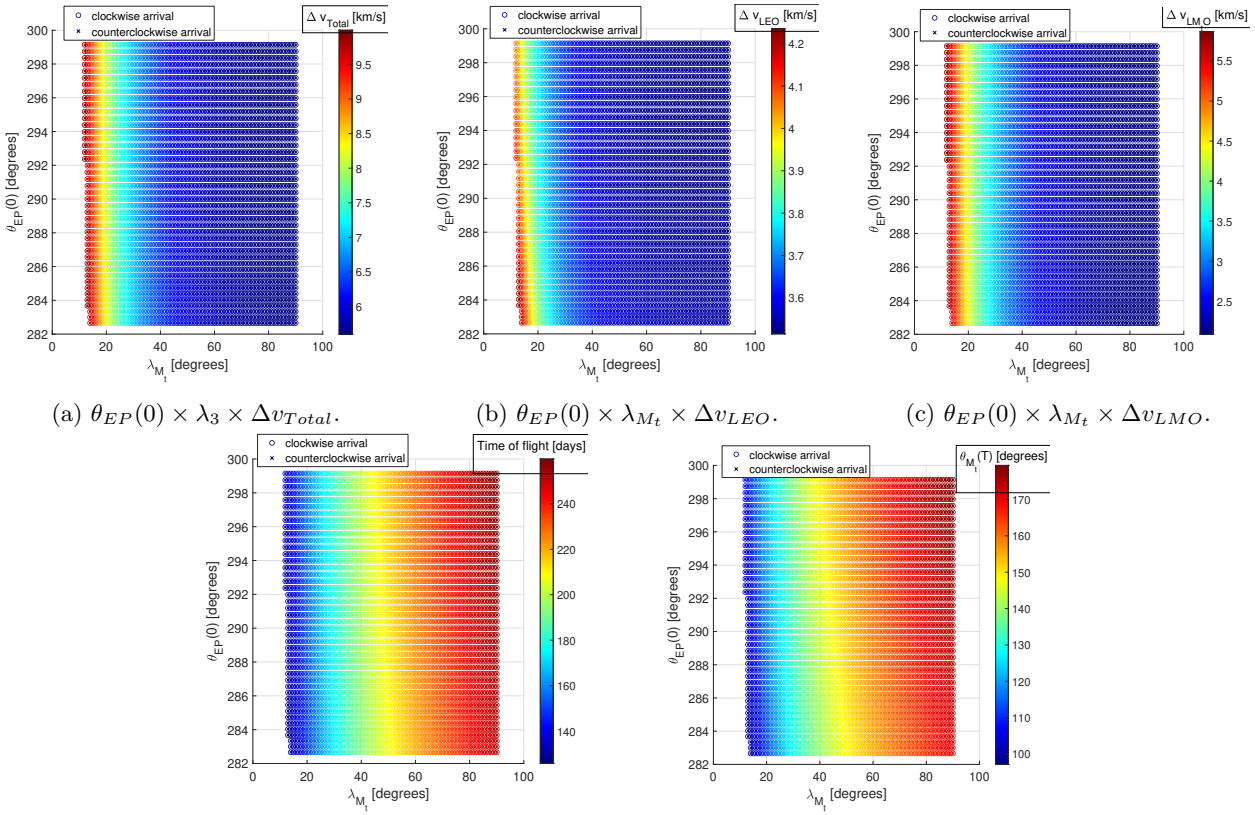

(a) $\theta_{EP}(0) \times \lambda_3 \times \Delta v_{Total}$. (b) $\theta_{EP}(0) \times \lambda_{M_t} \times \Delta v_{LEO}$. (c) $\theta_{EP}(0) \times \lambda_{M_t} \times \Delta v_{LMO}$.

(d) $\theta_{EP}(0) \times \lambda_{M_t} \times Time\ of\ flight$. (e) $\theta_{EP}(0) \times \lambda_{M_t} \times \theta_{M_t}(T)$.

Fig. 4. Main parameters of the patched-conic approximation with detailed geometry. Earth-Mars mission. The color figure can be viewed online.

about 720.824 m/s (Figure 4b), Δv_{LM_tO} can decrease 3.779155 km/s (Figure 4c). As for the Earth-Venus mission the decreasing of fuel consumption is due to both velocity increments: while Δv_{LEO} can decrease to about 1.258184 km/s (Figure 5b), Δv_{LVO} can decrease to 2.769650 km/s (Figure 5c). The decreasing of fuel consumption is strongly related to the angle λ_{Mt} for the Earth-Mars mission or λ_V for the Earth-Venus mission. To illustrate this fact, observe in Figures 4a and 5a that Δv_{Total} has small changes for same values of λ_{Mt} or λ_V. This same remark is also true for the time of flight and for the final phase angle of the destiny planet $\theta_{EP}(T)$ or $\theta_V(T)$. By comparing Figure 4a with Figure 4d, and Figure 5a with Figure 5d, one can conclude that the solutions of minimum consumption correspond to the trajectories with larger time of flight for both Earth-Mars and Earth-Venus missions. The main parameters of the solutions with the smallest fuel consumption are highlighted in Tables 3 and 4, and, the trajectories are plotted in Figures 6 and 7, in which the rendezvous angles are also shown. For the Earth-Mars mission the rendezvous angle, $\theta_{M_t}(0)$, is positive, i.e, Mars is ahead the Earth at t_0; and for the Earth-Venus mission the rendezvous angle $\theta_V(0)$, is negative, which means that Venus is behind the Earth at t_0.

Note that for all the trajectories with the smallest fuel consumption, the arrival at the SOI of the destiny planet is nearly parallel to the orbital motion of the destiny planet around the Sun; thus, the angles λ_{Mt} and λ_V are about 90° for an ahead arrival or −90° for an arrival trajectory from behind. Therefore, these smallest fuel consumption trajectories present an heliocentric phase close to the Hohmann transfer. One can also classify the quadrant of the arrival trajectory in the SOI of the destiny planet as illuminated or non illuminated by the Sun. In this way, the smallest fuel consumption trajectories for the Earth-Mars mission with counterclockwise and clockwise arrival occur, respectively, in the illuminated quadrant and in the non-illuminated quadrant (see Figure 8). Both trajectories have the same fuel consumption and the same value of λ_{M_t} and they are very close to each other. The only difference is the phase angle that defines the arrival

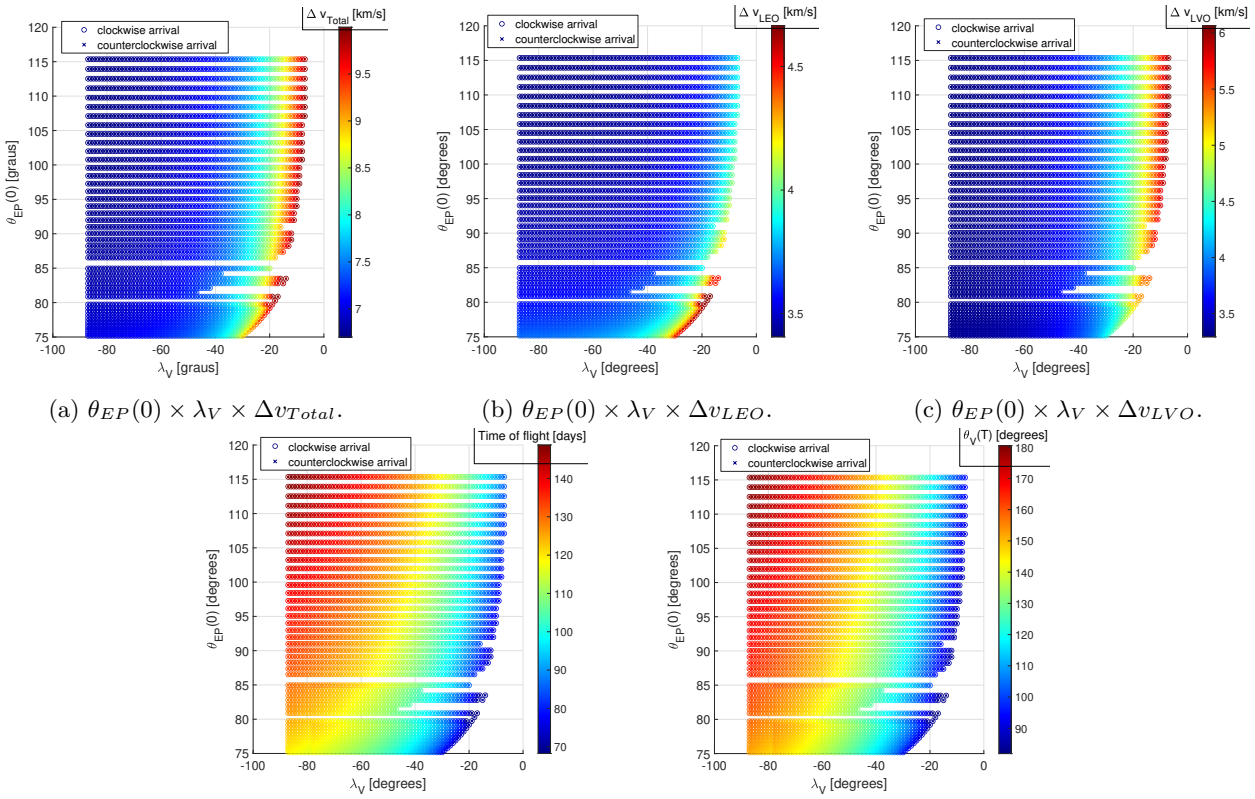

(a) $\theta_{EP}(0) \times \lambda_V \times \Delta v_{Total}$. (b) $\theta_{EP}(0) \times \lambda_V \times \Delta v_{LEO}$. (c) $\theta_{EP}(0) \times \lambda_V \times \Delta v_{LVO}$.

(d) $\theta_{EP}(0) \times \lambda_V \times Time\ of\ flight$. (e) $\theta_{EP}(0) \times \lambda_V \times \theta_V(T)$.

Fig. 5. Main parameters of the patched-conic approximation with detailed geometry. Earth-Venus mission. The color figure can be viewed online.

TABLE 3

MAIN PARAMETERS FOR THE SMALLEST FUEL CONSUMPTION TRAJECTORIES FOR EARTH-MARS MISSION

Model	Δv_{LEO} (km/s)	Δv_{LM_tO} (km/s)	Δv_{Total} (km/s)	Time of Flight (days)	$\theta_{M_t}(T)$ (degrees)	$\theta_{EP}(0)$ (degrees)
PCR4BP[1]	3.551905	2.100124	5.652029	257.861	179.075	298.382
Miele[2]	3.552000	2.100000	5.652000	257.880	179.020	298.150
Patched-conic based on Hohmann	3.555746	2.101260	5.657006	264.430	182.928	299.474
Patched-conic based on Gauss	3.555572	2.101454	5.657026	263.579	182.429	299.139
Patched-conic detailed geometry[3]	3.514668	2.087434	5.602101	257.965	179.353	297.573

[1] Results from a two degree-of-freedom optimization problem.

[2] Results based on the PR4CP calculated by Miele and Wang (1999b).

[3] Smallest fuel consumption trajectory found for $\lambda_{Mt} = 89^\circ$ (arrival ahead the SOI).

at the LM_tO (see Figure 8b). For the Earth-Venus mission, the results are inverted: the smallest fuel consumption trajectories with counterclockwise and clockwise arrival occur, respectively, in the non illuminated quadrant and in the illuminated quadrant (see Figure 9). Both trajectories have the same fuel

TABLE 4

MAIN PARAMETERS FOR THE SMALLEST FUEL CONSUMPTION TRAJECTORIES FOR EARTH-VENUS MISSION

Model	Δv_{LEO} (km/s)	Δv_{LVO} (km/s)	Δv_{Total} (km/s)	Time of Flight (days)	$\theta_V(T)$ (degrees)	$\theta_{EP}(0)$ (degrees)
PCR4BP[1]	3.449138	3.337284	6.786422	139.628	173.795	105.084
Patched-conic based on Hohmann	3.447245	3.339810	6.787055	151.822	189.273	115.420
Patched-conic based on Gauss	3.447417	3.339550	6.786967	151.771	189.197	115.355
Patched-conic detailed geometry [2]	3.406312	3.294024	6.700336	147.976	183.519	113.934

[1] Results from a two degree-of-freedom optimization problem.

[2] Smallest fuel consumption trajectory found for $\lambda_V = -87°$ (arrival behind the SOI).

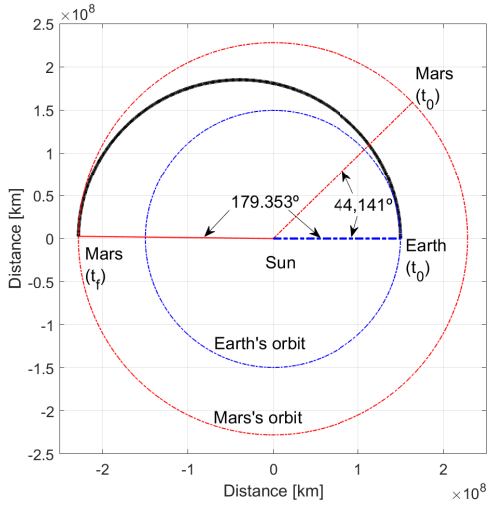

Fig. 6. Smallest fuel consumption trajectory for an Earth-Mars mission based on the patched-conic approximation. Arrival ahead the SOI of Mars. The color figure can be viewed online.

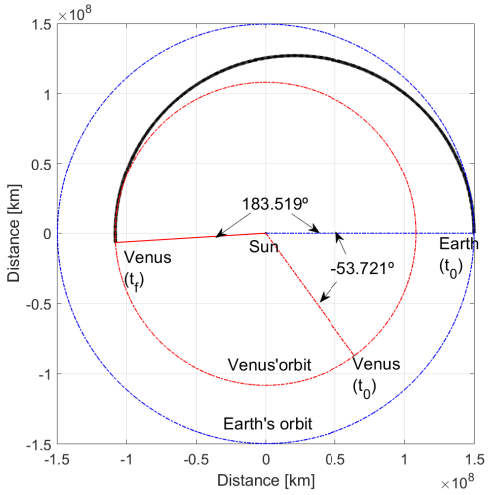

Fig. 7. Smallest fuel consumption trajectory for an Earth-Venus mission based on the patched-conic approximation. Arrival behind the SOI of Venus. The color figure can be viewed online.

consumption and the same value of λ_V. The only difference between them is the phase angle that defines the arrival at the *LVO* (see Figure 9b).

Therefore, in a real navigation problem for both Earth-Mars and Earth-Venus missions, one can define the direction of arrival at the final orbit when the space vehicle reaches the boundary of the SOI of the target planet because the clockwise and counterclockwise arrival trajectories are very close to each other.

Table 3 also shows the good agreement between the results for the smallest fuel consumption trajectory computed by: the patched-conic approximation; the optimal trajectory obtained by solving Problem 7 which is based on the PCR4BP; and the optimal results determined by Miele and Wang (1999b) for the Earth-Mars mission. Also, Tables 3 and 4 highlight the optimal results of the patched-conic based on the Gauss problem (Problem 2) and the results of the patched-conic based on the Hohmann transfer. For these last two models, the velocity increments are more compatible with the results provided by Miele and Wang (1999b) for the Earth-Mars mission (Table 3); however, a larger discrepancy occurs in the time of flight, which is 6 to 7 days longer than the one calculated by the PCR4BP. The detailed patched-conic approximation, on the other hand, presents

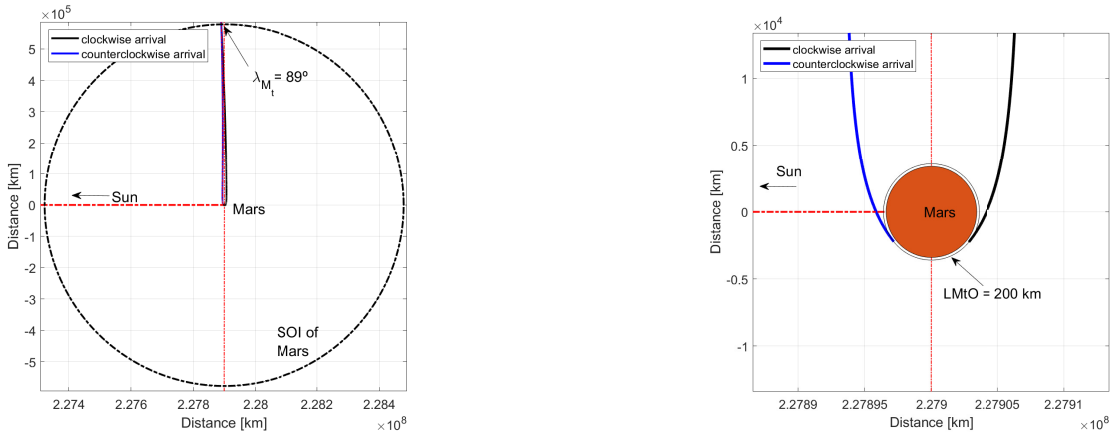

(a) Mars rotating reference frame. (b) Zoom at the LM_tO.

Fig. 8. Smallest fuel consumption trajectories with clockwise and counterclockwise arrivals at the LM_tO. The color figure can be viewed online.

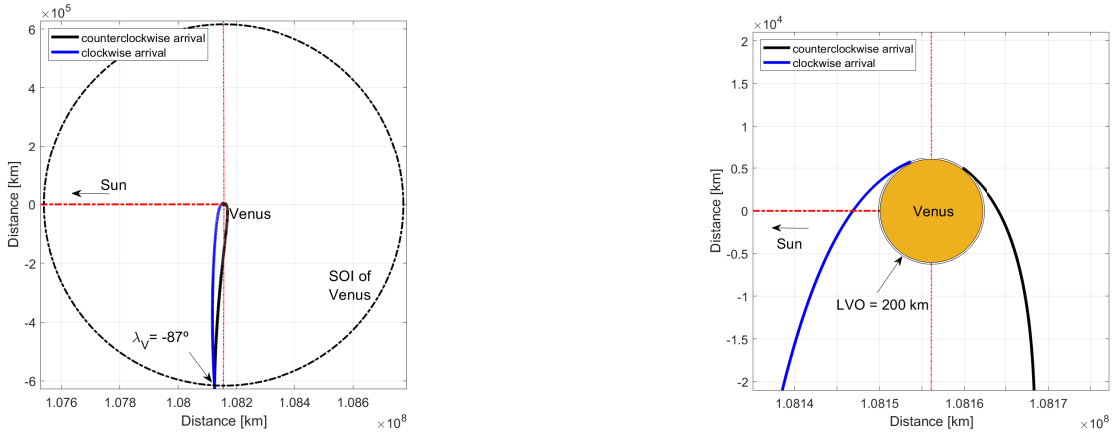

(a) Venus rotating reference frame. (b) Zoom at the LVO.

Fig. 9. Smallest fuel consumption trajectories with clockwise and counterclockwise arrivals at the LVO. The color figure can be viewed online.

values of time of flight, final phase angle $\theta_{M_t}(T)$, and, initial phase angle $\theta_{EP}(0)$ closer to the values of the model based on the PCR4BP.

In the Venus mission, the discrepancy of the time of flight is even greater, reaching 12 to 13 days when one compares the patched-conic based on Gauss or based the Hohmann transfer with the model based on the PCR4BP. Similar to the Earth-Mars mission, the detailed patched-conic approximation for the Earth-Venus mission presents values of time of flight, final phase angle $\theta_V(t)$, and initial phase angle $\theta_{EP}(0)$ closer to the values of the model based on the PCR4BP.

Therefore, even though the patched-conic approximation with detailed geometry presents a fuel consumption slightly different from the other models, it presents more detailed and accurate geometric information than the other patched-conic approximations (based on Gauss and based on the Hohmann transfer) allowing the visualization of the complete trajectory without discontinuity and with a time of flight compatible with the trajectory based on the PCR4BP. Moreover, one can include swing-by maneuver in this patched-conic approximation, whose results are presented later in this work.

3.1.2. *Planar Circular Restricted Three-Body Problem*

By now, one can use this patched-conic approximation to provide initial guesses for Problem 5 based on the PCR4BP. In this way, Figures 10 and 11 plot the fuel consumption determined by

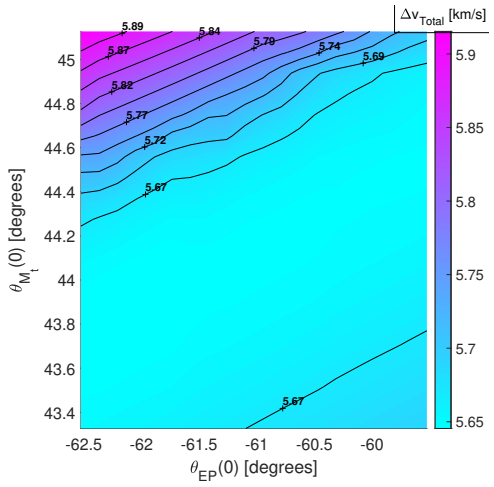

Fig. 10. Results of the TPBVP based on the PCR4BP for the Earth-Mars mission. The color figure can be viewed online.

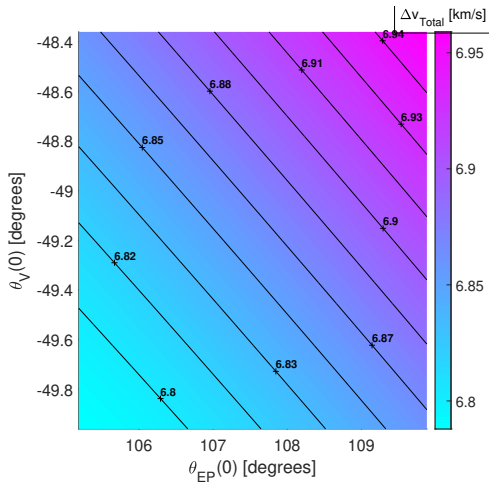

Fig. 11. Results of the TPBVP based on the PCR4BP for the Earth-Venus mission. The color figure can be viewed online.

the TPBVP (Problem 5) considering several sets of $\theta_{EP}(0), \theta_{M_t}(0)$, or $\theta_{EP}(0), \theta_V(0)$.

Figures 10 and 11 illustrate interpolated surfaces in which the results of Problem 5 are found, and, where one can observe that there is a minimum Δv_{Total} for each value of $\theta_{EP}(0)$. One can glimpse on Figures 10 and 11 that Δv_{Total} for the Earth-Venus mission is 1 km/s larger than the one of the Earth-Mars mission (see the color bars beside the figures). In order to determine the minimum consumption solutions in Figures 10 and 11, the one-degree optimization problem that prescribes $\theta_{M_t}(0)$, or $\theta_V(0)$, is solved (Problem 6). For this case, the results are shown in Figures 12 – 17.

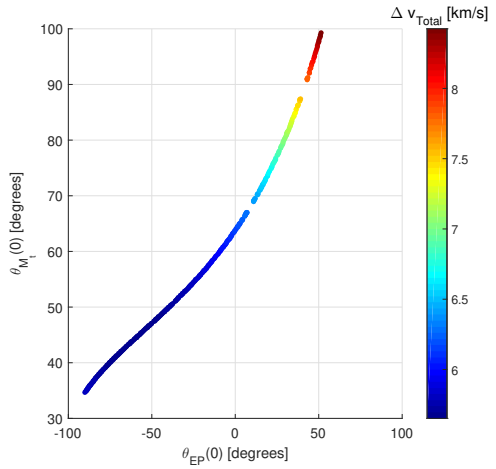

Fig. 12. Optimal curve $\theta_{EP}(0) \times \theta_{M_t}(0)$. Earth-Mars mission. The color figure can be viewed online.

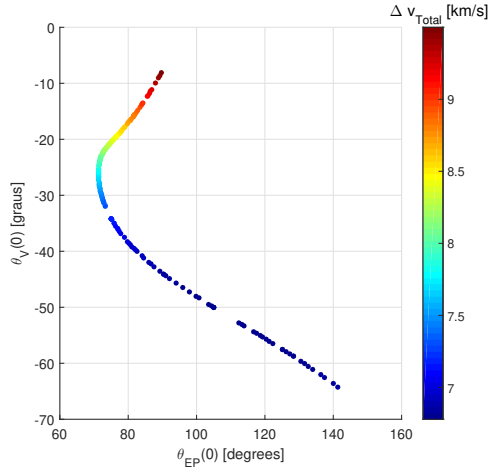

Fig. 13. Optimal curve $\theta_{EP}(0) \times \theta_{V_t}(0)$. Earth-Venus mission. The color figure can be viewed online.

Indeed, the rendezvous angles $\theta_{M_t}(0)$ and $\theta_V(0)$ have a huge influence on the fuel consumption. The proper choice of these angles can lead to a saving of fuel consumption of order of 3 km/s (or even greater) for both missions. Moreover, these angles define the initial phase angle of the space vehicle, $\theta_{EP}(0)$, and, consequently, the time of flight. Generally, for the Earth-Mars mission, the higher the angle $\theta_{M_t}(0)$, the higher the value of $\theta_{EP}(0)$ (Figure 12). The decreasing of $\theta_{EP}(0)$ is followed by the decreasing of the time of flight (Figure 14). Therefore, except for the trajectories with times of flight larger than 285 days approximately, the decreasing of the time of flight is followed by the decreasing of Δv_{Total}, which does not agree with the common sense that the time of flight must increase. On the other hand, for the Earth-Venus mission, the behavior of the parame-

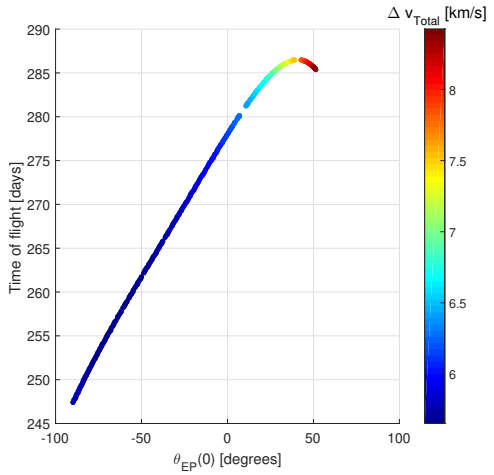

Fig. 14. Optimal curve $\theta_{EP}(0)\times$Time of flight. Earth-Mars mission. The color figure can be viewed online.

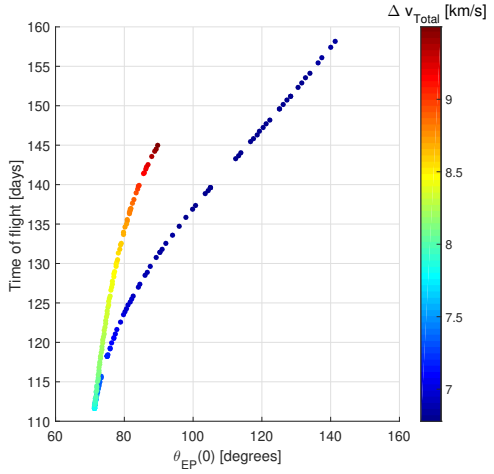

Fig. 15. Optimal curve $\theta_{EP}(0)\times$Time of flight. Earth-Venus mission. The color figure can be viewed online.

ters is inverted: the smaller the value of $\theta_V(0)$, the higher the angle $\theta_{EP}(0)$, for which Δv_{Total} is of order of 7 km/s (Figure 13). The increasing of $\theta_{EP}(0)$ is followed by an increasing of the time of flight (Figure 15), i.e, the decreasing of Δv_{Total} is achieved with an increasing of the time of flight, which agrees with common sense. A remark is necessary for the Earth-Venus trajectories that present larger Δv_{Total} (close to 8 km/s): for Δv_{Total} larger than 8 km/s, the trajectories obtained have increasing times of flight, reaching 145 days (Figure 15) with $\theta_V(0)$ increasing approximately until near $-10°$. This remark is better visualized in Figure 17, where an inversion of the curve behavior is observed for Δv_{Total}. All these behaviors are due to the two possibilities of solutions with approximately the same time of flight but with different fuel consumption. Figures 18 and 19 are an

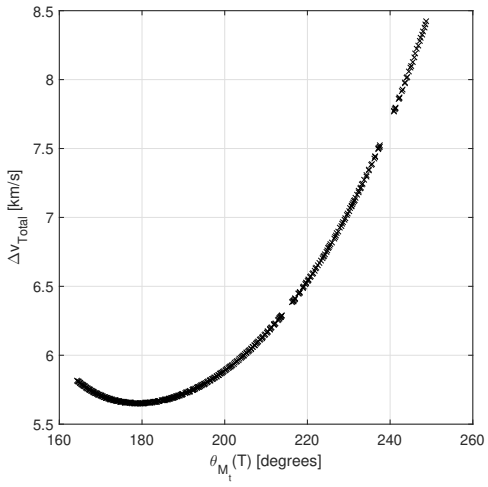

Fig. 16. Optimal curve $\theta_{M_t}(T) \times \Delta v_{Total}$. Earth-Mars mission. The color figure can be viewed online.

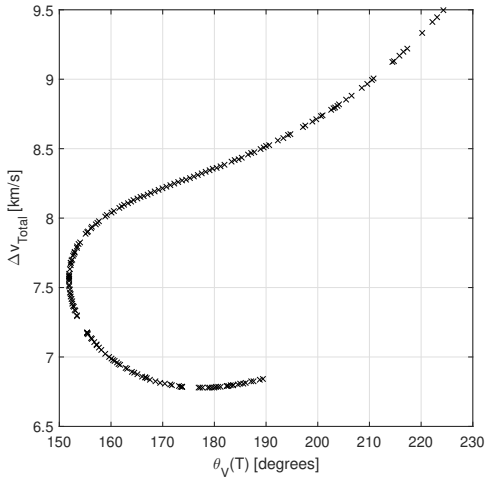

Fig. 17. Optimal curve $\theta_V(T) \times \Delta v_{Total}$. Earth-Venus mission.

example of these two possibility of trajectories: the trajectory in Figure 18 has a Δv_{Total} 2.218063 km/s larger than the one of Figure 19, but both present a time of flight of 139 days. Observe that the minimum fuel consumption trajectory of Earth-Venus mission has a value of $\theta_V(T)$ between 170° and 180° (Figure 17), and it is not the solution of minimum time, which is the singular point of the curve in Figure 15. This singular point (minimum time) makes the convergence of the two-degree of freedom optimization problem harder for the Earth-Venus mission because the numerical derivative expressions become sensitive. For the Earth-Mars, on the contrary, there is no singular point as the curve is well behaved in Figure 14. Moreover, the best optimal values of $\theta_{M_t}(T)$ and $\theta_V(T)$ are close to 180° (Figures 16 and 17).

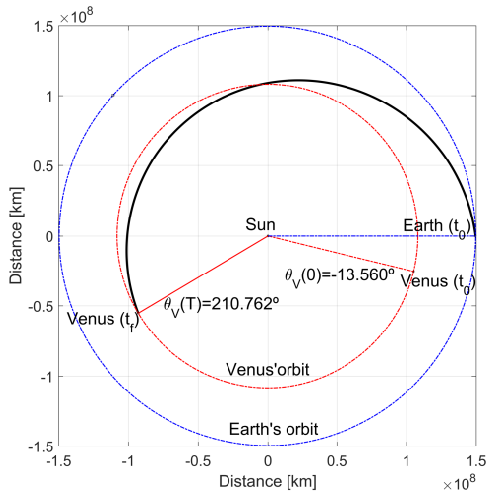

Fig. 18. Earth-Venus mission. Time of flight = 139.917 days, $\Delta v_{Total} = 9.004485$ km/s. The color figure can be viewed online.

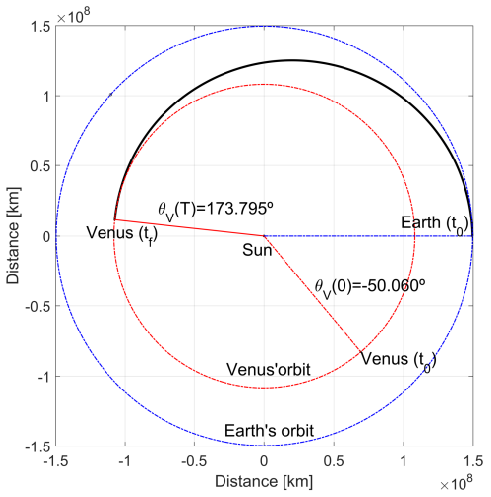

Fig. 19. Earth-Venus mission. Time of flight = 139.628 days, $\Delta v_{Total} = 6.786422$ km/s. The color figure can be viewed online.

In order to determine the best optimal initial phase angle of the destiny planet with higher accuracy, one can use the two-degree optimization problem (Problem 7) whose results have already been presented in Tables 3 and 4.

Note in Figure 6 that the value of the initial phase angle for the outer transfer means that the destiny planet is ahead of Earth ($\theta_{M_t}(0) > 0°$) with the initial position of the space vehicle underneath the line Sun-Earth ($180° < \theta_{EP}(0) < 360°$, Table 3). On the other hand, at the initial time of the inner transfer, the destiny planet is behind the Earth ($\theta_V(0) < 0°$), Figure 7, and the space vehicle is above the Sun-Earth line ($0° < \theta_{EP}(0) < 180°$, Table 4) for the minimum consumption trajectory.

The result of Problem 7 (based on the PCR4BP) for the Earth-Mars mission (Table 3) practically coincides with the result found by Miele and Wang (1999b), and it presents the optimal Δv_{Total} of nearly 50 m/s larger than the one of the patched-conic with detailed geometry. Despite this difference, the trajectories of these models are practically the same (Figure 20). The Mars rotating frame depicted in Figure 20d is a Sun centered reference frame with the X-axis pointing towards Mars at all times; thus, it rotates following the motion of Mars. For the Earth-Venus trajectory (Table 4), the optimal Δv_{Total} determined by Problem 7 (based on the PCR4BP) practically coincides with the one computed by the patched-conic approximation based on Hohmann and based on Gauss; however, the times of flight differ by nearly 12 days. By comparing the results of Problem 7 with the patched-conic with the detailed geometry, the difference in Δv_{Total} is about 86 m/s and the difference in time of flight is about 8.35 days with patched-conic approximation presenting the smaller fuel consumption and the larger time of flight for the Earth-Venus mission. This difference of results changes a little the shape of the trajectory as shown in Figure 21. The Venus rotating frame depicted in Figure 21d is a Sun centered reference frame with the X-axis pointing towards Venus at all time; thus, it rotates following the motion of Venus. For the Earth-Mars mission, however, the trajectories of both models coincide. The larger difference between the shapes of trajectories of the Earth-Venus mission occurs because this transfer problem is more sensitive as the orbital velocity of the target planet Venus is greater than the orbital velocity of the target planet Mars.

3.1.3. *Penalty on Fuel Consumption*

For more realistic models, in which one uses the ephemeris of the celestial bodies, it is not possible to find the proper geometrical set of the bodies in a given epoch that corresponds to the geometrical set of minimum fuel consumption determined by Problem 7 (two-degree of freedom optimization problem based on the PCR4BP). In this case, one can perform a correspondence of the geometrical set given by the ephemeris with a geometrical set determined by Problem 6 (one-degree of freedom optimization problem) by adjusting the initial phase angle of the destiny planet (rendezvous angle) in this last Problem. In this way, a penalty in the fuel consumption can be determined due to the deviations from the geometrical set determined by the two-degree of freedom

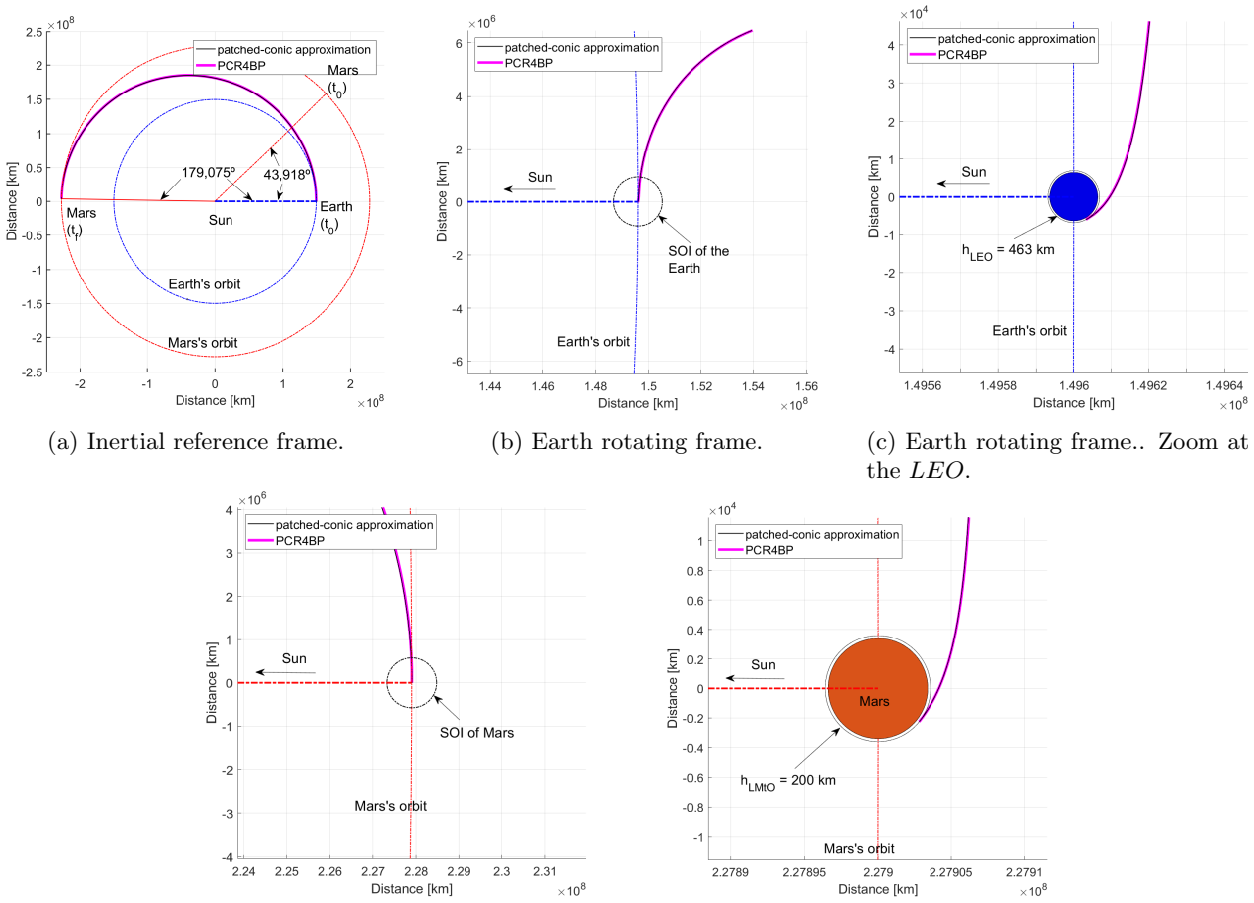

(a) Inertial reference frame.

(b) Earth rotating frame.

(c) Earth rotating frame.. Zoom at the LEO.

(d) Mars rotating frame.

(e) Mars rotating frame. Zoom at LM_tO.

Fig. 20. Optimal Earth-Mars trajectory. Phase angles are computed by PCR4BP. The color figure can be viewed online.

TABLE 5

PENALTY IN THE MAIN PARAMETERS DUE TO EARLY AND DELAYED DEPARTURES. EARTH-MARS MISSION

$\theta_{M_t}(0) - \theta_{M_t}(0)^*$	$(-)9.0°$	$\theta_{M_t}(0)^* = 43.918°$	$(+)15.0°$	$(+)30.0°$	$(+)40.0°$
Δv_{LEO} (km/s)	$(+)0.123037$	3.551905	$(+)0.240781$	$(+)0.800470$	$(+)1.306203$
Δv_{LM_tO} (km/s)	$(+)0.036667$	2.100124	$(+)0.058534$	$(+)0.200583$	$(+)0.340452$
Δv_{Total} (km/s)	$(+)0.159705$	5.652029	$(+)0.299315$	$(+)1.001053$	$(+)1.646655$
Time ($days$)	(-)10.417	257.861	$(+)16.377$	$(+)25.752$	$(+)28.356$
$\theta_{EP}(0)$ ($degrees$)	(-)28.055	298.382	$(+)49.801$	$(+)81.454$	$(+)96.600$

optimization problem. Figures 22a and 22b show the penalty in Δv_{Total}, respectively, for the Earth-Mars and Earth-Venus missions, when the rendezvous angle does not agree with its optimal value, denoted by the subscript $*$. The resulting change in the time of flight due to this advance or delay of the rendezvous angle is shown in Figures 22c and 22d, and the launch window, which is defined by the variation of $\theta_{EP}(0)$, is visualized in Figures 22e and 22f. Note that the curves highlighted by Figure 22 are the results of the one-degree of freedom optimization problem (Problem 6). Tables 5 and 6 exemplify some points of Figure 22 to better quantify the penalty on the parameters due to advance or delay of the ren-

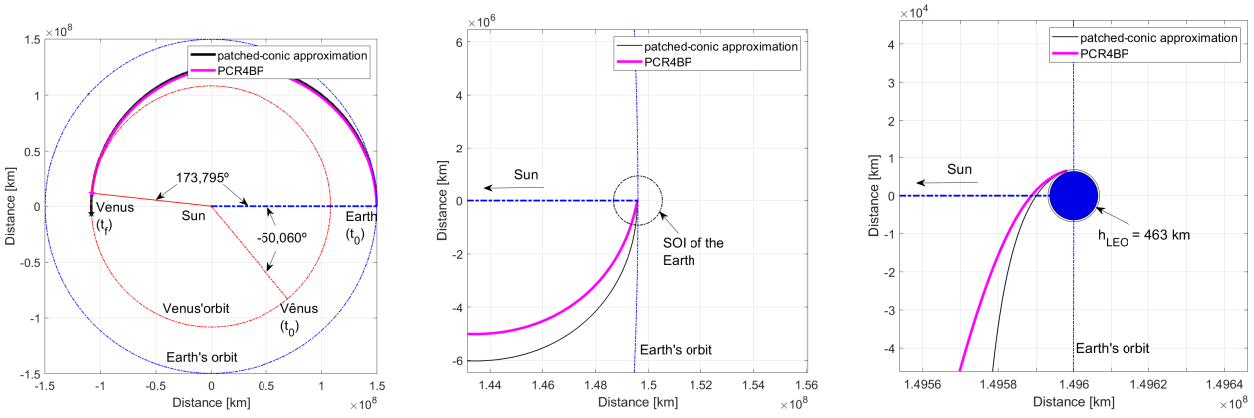

(a) Inertial reference frame.

(b) Earth rotating frame.

(c) Earth rotating frame.. Zoom at the LEO.

(d) Venus rotating frame.

(e) Venus rotating frame. Zoom at LM_tO.

Fig. 21. Optimal Earth-Venus trajectory. Phase angles are computed by PCR4BP. The color figure can be viewed online.

TABLE 6

PENALTY IN THE MAIN PARAMETERS DUE TO EARLY AND DELAYED DEPARTURES. EARTH-VENUS MISSION

$\theta_V(0) - \theta_V(0)^*$	$(-)9.0°$	$\theta_V(0)^* = -50.060°$	$(+)15.0°$	$(+)30.0°$	$(+)40.0°$
Δv_{LEO} (km/s)	(+)0.013842	3.449138	(+)0.278435	(+)0.752205	(+)0.643154
Δv_{LVO} (km/s)	(+)0.002513	3.337284	(+)0.063947	(+)0.835651	(+)1.901170
Δv_{Total} (km/s)	(+)0.016355	6.786422	(+)0.342381	(+)1.587856	(+)2.544324
Time ($days$)	(+)12.731	139.628	(-)20.312	(-)14.062	(+)3.935
$\theta_{EP}(0)$ ($degrees$)	(+)25.454	105.084	(-)29.212	(-)29.382	(-)17.101

dezvous phase angle. The following comments are noted for these results:

1. Positive values of $\theta_{M_t}(0) - \theta^*_{M_t}(0)$, which are denoted by (+) for the Earth-Mars mission indicate early departures of the space vehicle from the LEO, while negative values, which are denoted by (-), indicate delayed departures. For the Earth-Venus mission, positive values of $\theta_V(0) - \theta^*_V(0)$ indicate delayed departures, and negative values indicate early departures.

2. Both delayed and early departures in both missions increase the fuel consumption: an early departure corresponding to a change in the rendezvous angle of 40° in the Earth-Mars mission increases Δv_{Total} in 1.646566 km/s (Ta-

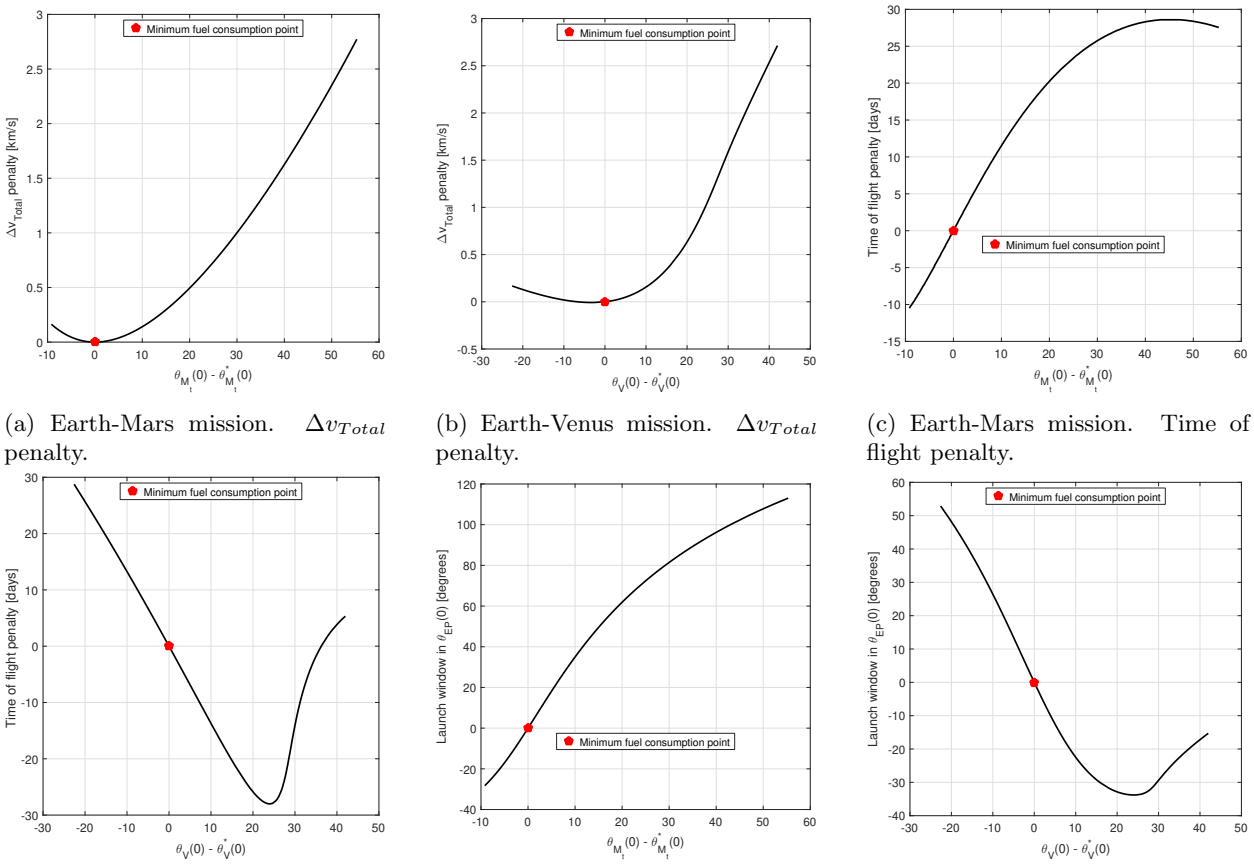

(a) Earth-Mars mission. Δv_{Total} penalty.

(b) Earth-Venus mission. Δv_{Total} penalty.

(c) Earth-Mars mission. Time of flight penalty.

(d) Earth-Venus mission. Time of flight penalty.

(e) Earth-Mars mission. $\theta_{EP}(0)$ penalty.

(f) Earth-Venus mission. $\theta_{EP}(0)$ penalty.

Fig. 22. Penalty in the main parameters with respect to minimum fuel consumption trajectory (Problem 7). The color figure can be viewed online.

ble 5), while a delayed departure corresponding to the same value of the rendezvous angle in the Earth-Venus mission increases Δv_{Total} by 2.544324 km/s (Table 6). The increase in Δv_{Total} is an effect of the increase of both velocity increments Δv_{LEO} and Δv_{LM_tO} or Δv_{LVO} (Tabs. 5 and 6). For the Earth-Venus mission (Table 6), there is a slight decrease of Δv_{LEO} between the delayed departures corresponding to a variation of the rendezvous angle of 30° and 40°; however, Δv_{LVO} more than doubles its value culminating in an significant increase of Δv_{Total}.

3. The early departures for the Earth-Mars mission $(\theta_{M_t}(0) - \theta^*_{M_t}(0) > 0)$ and for the Earth-Venus mission $(\theta_V(0) - \theta^*_V(0) < 0)$ increase the time of flight (see Figures 22c and 22d). For example, the early departure corresponding to a variation of the rendezvous angle of 15° for the Earth-Mars mission increases the time of flight by 16.377 days with a penalty on Δv_{total} of 299.315 m/s (Table 5); and the delayed departure corresponding to a variation of the rendezvous angle of −9° for the Earth-Venus mission increases the time of flight by 12.731 days with a penalty on Δv_{total} of 16.355 m/s (Table 6).

4. Delaying the departure for both Earth-Mars and Earth-Venus mission decreases the time of flight; however, there is a delayed departure that minimizes the time of flight in the Earth-Venus mission. Observe in Table 6 that a delayed departure corresponding to a variation of the rendezvous angle of 15° for the Earth-Venus mission decreases the time of flight by 20.312 days with a penalty on Δv_{total} of 342.381 m/s, while a delayed departure of 40° for the same mission increases the time of flight by 3.935 days, with a penalty on Δv_{total} of 2544.324 m/s, which shows that there is a minimum time of flight.

5. The launch window, which is defined by the change in $\theta_{EP}(0)$, is larger for the Earth-Mars mission: assuming a variation of the rendezvous angles within the interval of $-10°$ and $40°$, the launch window for the Earth-Mars mission is, approximately, between $-30°$ and $100°$ (angular range of $130°$). On the other hand, for the Earth-Venus mission, the launch window is defined between $-35°$ and $25°$ (angular range of $60°$) for the same variation of the rendezvous angle. As an example, the early departure of the space vehicle corresponding to a variation of the rendezvous angle of $30°$ increases $\theta_{EP}(0)$ by $81.454°$ (Table 5) for the Earth-Mars mission and decreases $\theta_{EP}(0)$ by only $29.382°$ (Table 6) for the Earth-Venus mission.

In general, by observing Figures 22, delayed and early departures increase the fuel consumption (Figures 22a and 22b) in both missions; however, the minimum fuel consumption solution for the Earth-Venus mission lies on a flatter region of the Δv_{Total} penalty curve (Figure 22b) than the one for the Earth-Mars mission (Figure 22a) making the optimization algorithm convergence harder. The minimum fuel consumption solution for both missions does not correspond to the maximum or minimum time of flight solution (Figure 22c and Figure 22d); moreover, the Earth-Mars mission presents a maximum time of flight solution (Figure 22c) in contrast to the Earth-Venus mission, which presents a minimum time of flight solution (Figure 22d). Finally, the launch window is larger for the Earth-Venus mission, as already discussed (Figure 22e and Figure 22f).

The penalty on the main parameters for the Earth-Mars mission was also observed by Miele and Wang (1999b); part of their results are given in Table 7. A good agreement is observed between the results of Table 5 and the ones of Table 7. This fact is better observed in the columns with $\theta_{M_t}(0) - \theta^*_{M_t}(0) > 0$; the values practically coincide.

The next section studies the possibility of saving fuel consumption without increasing significantly the time of flight for both missions, Earth-Mars and Earth-Venus, by including a lunar swing-by maneuver.

3.2. *Interplanetary Missions with Swing-by Maneuver*

Firstly, this section studies the solutions of interplanetary trajectories for Earth-Mars and Earth-Venus missions by solving only the TPBVPs with a lunar swing-by maneuver (Problems 4 and 8). Next, the optimal solutions of the three-degree of freedom optimization problem (Problem 9) are presented.

3.2.1. *Non-Optimal Solutions*

Tables 8 and 9 compare the interplanetary trajectories for Earth-Mars and Earth-Venus missions with lunar swing-by maneuvers. The results of the patched-conic approximation with detailed geometry (Problem 4) that includes a lunar swing-by maneuver, Table 8, have already explained by Gagg Filho and da Silva Fernandes (2018). These results are used as initial guess to solve the TPBVP defined by Problem 8 in the context of the PCR5BP, which is highlighted in Table 9. In this last model, the gravitational attraction of the Moon is neglected during the interplanetary and planetocentric phases. If the initial condition for Problem 8 is accurate enough, the lunar swing-by maneuver will occur naturally during the integration of the equations of motion (equations 41 and 42).

By comparing both models that include the lunar swing-by maneuver, i.e., the patched-conic approximation and the PCR5BP, a difference is observed between the results of Table 8 and Table 9: the patched-conic approximation presents a fuel consumption, Δv_{Total}, distinct from the one of the PCR5BP. For the Earth-Venus mission, for instance, the trajectory based on the patched-conic approximation has Δv_{Total} about 224.373 m/s smaller than the one of the trajectory based on the PCR5BP. This difference between models has been already observed for the interplanetary missions without swing-by maneuvers (Table 4), where this difference reaches 86.086 m/s. This discrepancy between the models is also observed for the Earth-Mars mission with lunar swing-by: the trajectory based on the patched-conic approximation presents a Δv_{Total} about 121.718 m/s smaller than the one of the trajectory based on the PCR5BP. For the Earth-Mars mission without swing-by maneuver, this difference is 50 m/s (Table 3).

In the context of the patched-conic approximation, the Earth-Mars mission with a lunar swing-by (Table 8) shows a saving of fuel consumption of 153 m/s with approximately the same time of flight as the one of the patched-conic without lunar swing-by maneuver; and the Earth-Venus mission presents a saving of fuel consumption of 33.21 m/s with a time of flight only 1.5 days larger than the one of the patched-conic without lunar swing-by maneuver. The results in the context of the PCR5BP only reinforce these remarks: the Earth-Mars mission with lunar swing-by shows a saving of fuel consumption

TABLE 7

PENALTY IN THE MAIN PARAMETERS DUE TO EARLY AND DELAYED DEPARTURES (MIELE & WANG 1999b). EARTH-MARS MISSION

$\theta_{M_t}(0) - \theta_{M_t}(0)^*$	$(-)14.86^\circ$	$\theta_{M_t}(0)^* = 43.860^\circ$	$(+)15.14^\circ$	$(+)30.14^\circ$
Δv_{LEO} (km/s)	(+)0.341	3.552	(+)0.240	(+)0.803
Δv_{LM_tO} (km/s)	(+)0.127	2.100	(+)0.058	(+)0.201
Δv_{Total} (km/s)	(+)0.468	5.652	(+)0.298	(+)1.004
Time (*days*)	(-)13.29	257.88	(+)16.48	(+)25.74
$\theta_{EP}(0)$ (*degrees*)	(-)37.73	298.15	(+)49.97	(+)81.80

TABLE 8

MINIMUM FUEL CONSUMPTION SOLUTION*

Parameter	Earth-Mars	Earth-Venus
Δv_{LEO} (km/s)	3.362211	3.376566
Δv_{LMtO} or Δv_{LVO} (km/s)	2.086891	3.289849
Δv_{Total} (km/s)	5.449101	6.666415
Time of flight (days)	257.443	149.440
$\theta_E(0)$ (degrees)	-46.188	86.040
Rendezvous angle (degrees)	43.368	-56.269
$\theta_{M_t}(T)$ or $\theta_V(T)$ (degrees)	132.079	269.358
h_{sP} (km)	1400.0	9100.0
$\theta_{EP}(0)$ (degrees)	-141.035	-151.321
λ_1 (degrees)	-17.0	4.0
λ_S (degrees)	91.845	90.170
λ_{M_t} or λ_V	90.0	-90.0

*Patched-conic approximation with a lunar swing-by maneuver.

of 81.21 m/s with a time of flight only 0.418 days smaller than the mission without lunar swing-by maneuver (PCR4BP); and the Earth-Venus mission with lunar swing-by presents a fuel consumption of 104.366 m/s smaller than the one without swing-by maneuver (PCR4BP) with a time of flight only 1.931 days larger than the mission without lunar swing-by maneuver.

This comparison using Table (8) and Table (9) is limited because, even considering different models, they do not shown exactly the same trajectory. The only correspondence between Tables (8) and Table (9) is that the result of trajectory of Table (8) is used to glimpse an initial guess to solve the TPBVP (Problem 8), whose solutions are presented in Table (9). During the convergence of the algorithm that solves this TPBVP, the solution can move away from the initial guess. A better comparison can be made if an optimization problem is solved considering both models; however, the intention of this paper is to illustrate that the patched-conic approximation with lunar swing-by maneuver can be well utilized as an initial guess for the model based on the PCR5BP. Since the objective of this paper is also to study the saving of fuel consumption due to the lunar swing-by maneuver on interplanetary missions, and, considering that there is a potential of saving fuel consumption as illustrated in Table (9), the optimization problem with a three-degree of freedom is conducted to obtain more solid conclusions.

Figures 23 and 24 plot the trajectories described by Tables 8 and 9. Since the trajectories based on the PCR5BP are obtained by solving Problem 8, there is no intermediary constraint that defines the swing-by maneuver, which appears naturally from the integration of the equations of motion. Due to this absence of an intermediary constraint on the PCR5BP and due to the dynamic difference of the models, the swing-by maneuver can be changed by the Newton-Raphson method in order to converge. In other words, since there is no intermediary constraint prescribing the lunar swing-by maneuver, the Newton-Raphson method does not take into consideration what happens during the trajectory as long as the final constraints are satisfied, so the occurrence of the lunar swing-by maneuver on the PCR5BP essentially depends on the initial guess that defines the departure at the LEO.

This fact is better visualized on the Earth-Venus mission, Figure 23e, where the space vehicle performs a lunar swing-by maneuver in the context of the PCR5BP with a periselenium altitude smaller than the one of the patched-conic approximation. On the other hand, for the Earth-Mars mission, the initial guess for solving Problem 8 is so accurate that the periselenium altitude of the lunar swing-by maneuver based on the PCR5BP practically coincides with the prescribed altitude of the patched-conic approximation (Figure 24e); however, an overview of the complete trajectory (Figure 23a and Figure 23b), departure geometry (Figure 23c), and arrival geometry (Figure 23d) reveal that the shapes of the tra-

TABLE 9

SOLUTION FOR INTERPLANETARY MISSIONS*

Parameters	Earth-Mars	Earth-Venus
Δv_{LEO} (km/s)	3.469766	3.426035
Δv_{LMtO} or Δv_{LVO} (km/s)	2.101053	3.464753
Δv_{Total} (km/s)	5.570819	6.890788
Time of flight (days)	257.443	142.697
$\theta_E(0)$ (degrees)	0.0	0.0
Rendezvous angles (degrees)	41.605566	-42.836
$\theta_{M_t}(T)$ or $\theta_V(T)$ (degrees)	176.544391	185.939
$\theta_{EP}(0)$ (degrees)	-88.194	76.505
$\theta_M(0)$ (degrees)	43.940	209.472

*With lunar swing-by maneuver in the context of the PCR5BP.

jectories are different. A disagreement between the trajectories of different models is also observed for the Earth-Venus mission (Figure 24). Indeed, these differences are already expected, as explained before by Tables 8 and 9. For both missions, the visualization of trajectories in the inertial reference frame centered at the Sun of both models must be done in distinct figures since the x-axis of the inertial reference frame is not the same: the x-axis of the inertial reference frame used in context of the PCR5BP (Figure 23b and Figure 24b) is the Sun-Earth direction at $t = t_0$; on the other hand, the x-axis of the inertial reference frame used for the patched-conic approximation with lunar swing-by (Figure 23a and Figure 24a) is parallel to the direction Earth-Moon at $t = t_0$. Therefore, the comparison of the trajectories is performed by considering the relative positions of the bodies and rotating reference frames. In order to help this comparison, Figures 23a, 23b, 24a, and 24b highlight the rendezvous angles and the angles that define the arc of the complete trajectory. In Figures 23e and 24e, the comparison of trajectories is straightforward since both are shown in the Moon rotating reference frame. This reference frame is centered on Earth with the X-axis pointing towards the Moon at all time, so that it rotates following the orbital motion of the Moon around Earth; and the Y-axis is orthogonal to the X-axis in the plane of motion of the bodies. In these last figures, the changing from the inertial reference frame centered on the Sun (Figures 23a, 24a) to the Moon rotating reference frame centered on the Earth (Figures 23e, 24e) amplifies the characterization of the phases of the patched-conic approximation, in a way that sharper corners are observed.

3.2.2. *Optimal Solutions: The Three-Degree of Freedom Optimization Problem*

In order to obtain better conclusions about the fuel consumption and the time of flight for the Earth-Mars and Earth-Venus missions with an intermediary lunar swing-by maneuver, the three-degree of freedom optimization problem (Problem 9) is solved in the context of the PCR5BP, in which the parameters $\theta_{EP}(0)$, $\theta_{M_t}(0)$, and $\theta_M(0)$ are set as unknown to solve the problem.

As mentioned, all the optimization problems in this work are solved by means of the Sequential-Gradient Restoration Algorithm (SGRA) (Miele et al. 1969) for constrained functions. In this section, this algorithm is initialized using a solution of the TPBVP defined by Problem 8; the results are presented in Table 9. The first step of the SGRA is the gradient phase, i.e, an perturbation is induced in the initial point, given by the initial guess, in the direction opposite to the gradient of the function to be minimized, i.e., in the direction to decrease the fuel consumption to obtain a new point. After, this first gradient phase, a restoration phase is performed in order to restore this new point to satisfy the constraints. The gradient and restoration are applied sequentially until the tolerance of the function to be minimized is achieved. Therefore, after each restoration phase there is a solution of the TPBVP with decreasing fuel consumption. Figures 25 and 27 show the solution after each restoration phase for Earth-Mars and Earth-Venus, respectively.

Since there is no constraint that specifies the periselenium altitude, the SGRA eventually can determine trajectory solutions in which the space vehicle collides with the Moon. Thus, the solutions with decreasing fuel consumption in Figures 25 and 27 are classified as trajectories that collide and trajectories that do not collide with the Moon. For the Earth-Mars mission, the first solutions of the SGRA do not collide with the Moon (Figure 25). As the fuel consumption decreases, the solutions collide until they reach the minimum fuel consumption at 5.352415 km/s, a decrease of 218.404 m/s. The initial phase angle of the Moon decreases by about 46.008° (Figure 25a), the rendezvous angle increases about 4.515° (Figure 25c), and the initial phase angle of the space vehicle decreases about 48.743° (Figure 25d). The time of flight, however, almost does not change during the optimization algorithm, staying at 257.443 days (Figure 25b). In a practical way, the interesting solution is the one that does not collide with the Moon, which is indicated by the red arrow in Figure 25; results are highlighted in Ta-

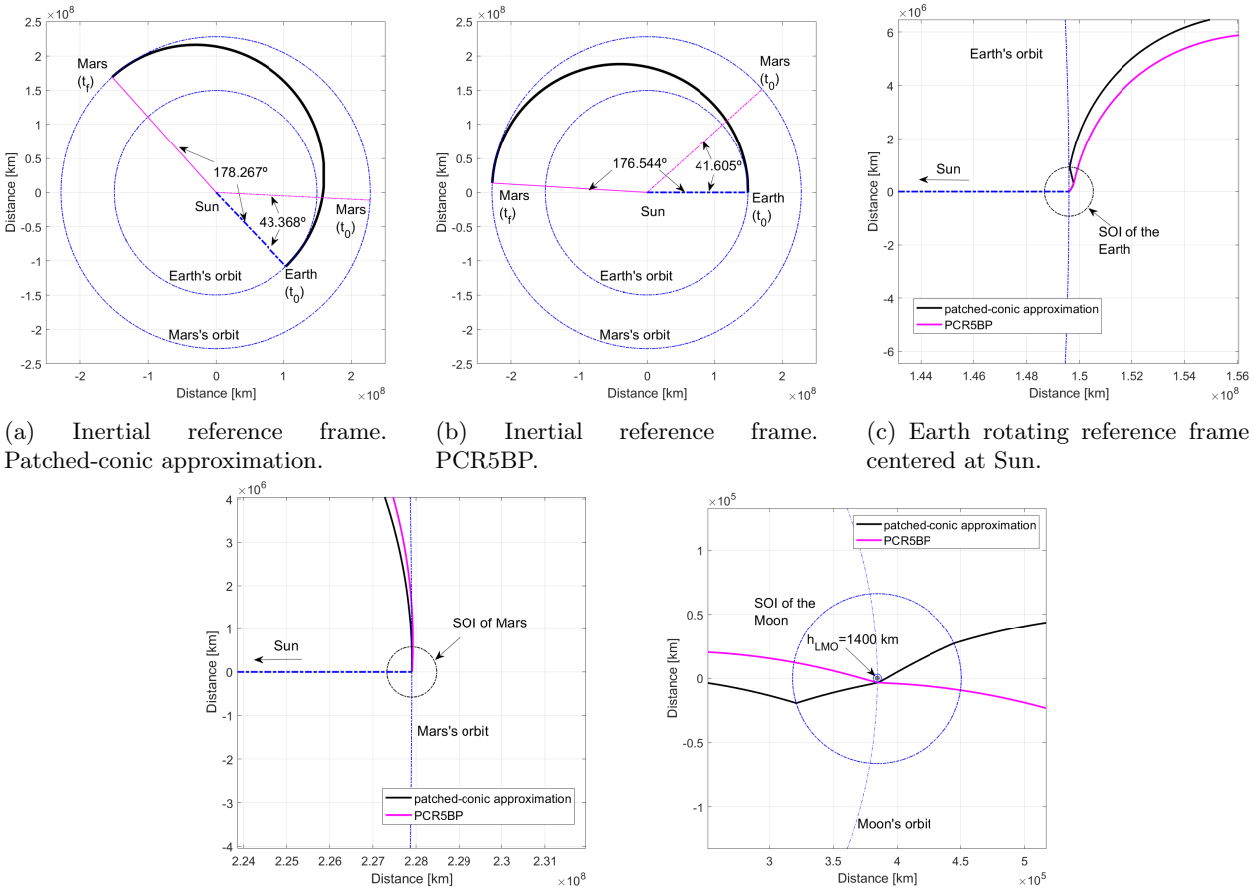

(a) Inertial reference frame. Patched-conic approximation.

(b) Inertial reference frame. PCR5BP.

(c) Earth rotating reference frame centered at Sun.

(d) Mars rotating reference frame centered at Sun.

(e) Moon rotating reference frame centered at Earth. h_{LMO} is the periselenium altitude of the swing-by maneuver.

Fig. 23. Earth-Mars mission with a lunar swing-by maneuver. The color figure can be viewed online.

TABLE 10

MAIN PARAMETERS FOR THE SMALLEST FUEL CONSUMPTION TRAJECTORIES FOR EARTH-MARS MISSION WITH AND WITHOUT A LUNAR SWING-BY MANEUVER

Model	Δv_{LEO} (km/s)	Δv_{LM_tO} (km/s)	Δv_{Total} (km/s)	Time of Flight (days)	$\theta_{M_t}(T)$ (degrees)	$\theta_{EP}(0)$ (degrees)	$\theta_{M_t}(0)$ (degrees)
PCR4BP[1]	3.551905	2.100124	5.652029	257.861	179.075	298.382	43.918
PCR5BP[2]	3.404922	2.098633	5.503555	257.443	180.425	270.881	45.486

[1] Results from the two degree-of-freedom optimization problem based on the PCR4BP.

[2] Results from the two degree-of-freedom optimization problem based on the PCR5BP without a collision with the Moon.

ble 10 in comparison to the solution based on the PCR4BP. Therefore, the design of a lunar swing-by maneuver for the Earth-Mars mission saves up to 148.174 m/s of fuel consumption without changes on the time of flight, which stays at 257 days, and without many changes in the rendezvous angle, which increases only 1.568° (Table 10). The result of the trajectory without a collision with the Moon is, actu-

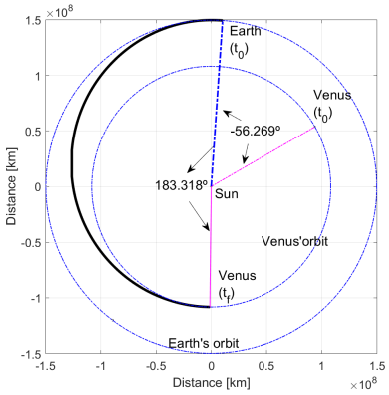

(a) Inertial reference frame. Patched-conic approximation.

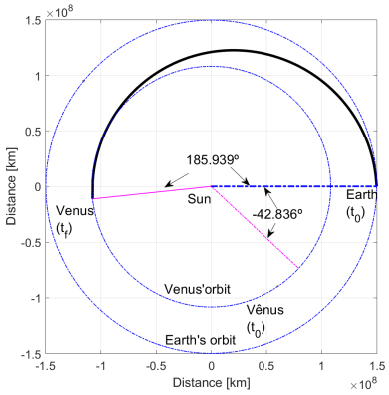

(b) Inertial reference frame. PCR5BP.

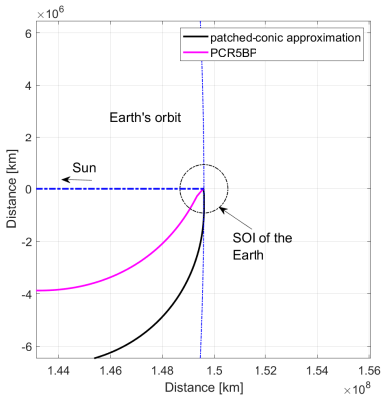

(c) Earth rotating reference frame centered at Sun.

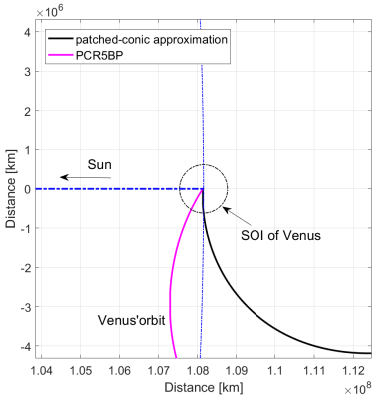

(d) Mars rotating reference frame centered at Sun.

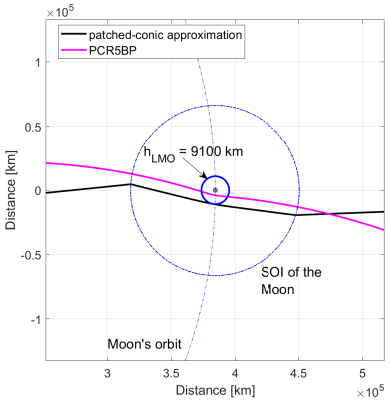

(e) Moon rotating reference frame centered at Earth. h_{LMO} is the periselenium altitude of the swing-by maneuver.

Fig. 24. Earth-Venus mission with a lunar swing-by maneuver. The color figure can be viewed online.

ally, a sub-optimal result extracted from the convergence of the optimization algorithm; thus, the same optimization problem applied to a different initial trajectory can lead to another sub-optimal trajectory. By observing Figures 25a, 25d, and Figure 25c the departure geometry must be accurate; otherwise, the space vehicle will collide to the Moon. By considering a window for the rendezvous angle of only 3.881° where the solutions without collision belong, Figure 25c, a maximum penalty on the fuel consumption of 67.264 m/s is observed.

Figure 26 plots three Earth-Mars trajectories with lunar swing-by maneuver: the first one is used as the initial guess to initialize the SGRA (magenta color); the second one is the optimal solution determined by the SGRA (black color); and, the third one is the trajectory determined by the SGRA with the smaller fuel consumption without a collision with the Moon (green color). The changing of the trajectory shape at departure from the Earth's SOI (Figure 26a) is well visualized and it is due to the convergence of the SGRA. The smaller fuel consumption trajectory without a collision with the Moon (green trajectory) is closer to the optimal trajectory (magenta) than the initial guess trajectory (magenta). In fact, the trajectory without collision and the optimal trajectory perform an intense swing-by maneuver, which is better visualized in Figure 26b. Note that, as trajectories with smaller fuel consumption are obtained by SGRA, the distance of the periselenium is smaller on the swing-by maneuver, which has great influence on the deflection of the trajectory. Thus, the greater the deflection the smaller is the fuel consumption. For the trajectory without collision with the Moon, the altitude of the periselenium is just 78.313 km. On the other hand, the shape of the optimal trajectory and the shape of the non-collision trajectory with the Moon at the arrival

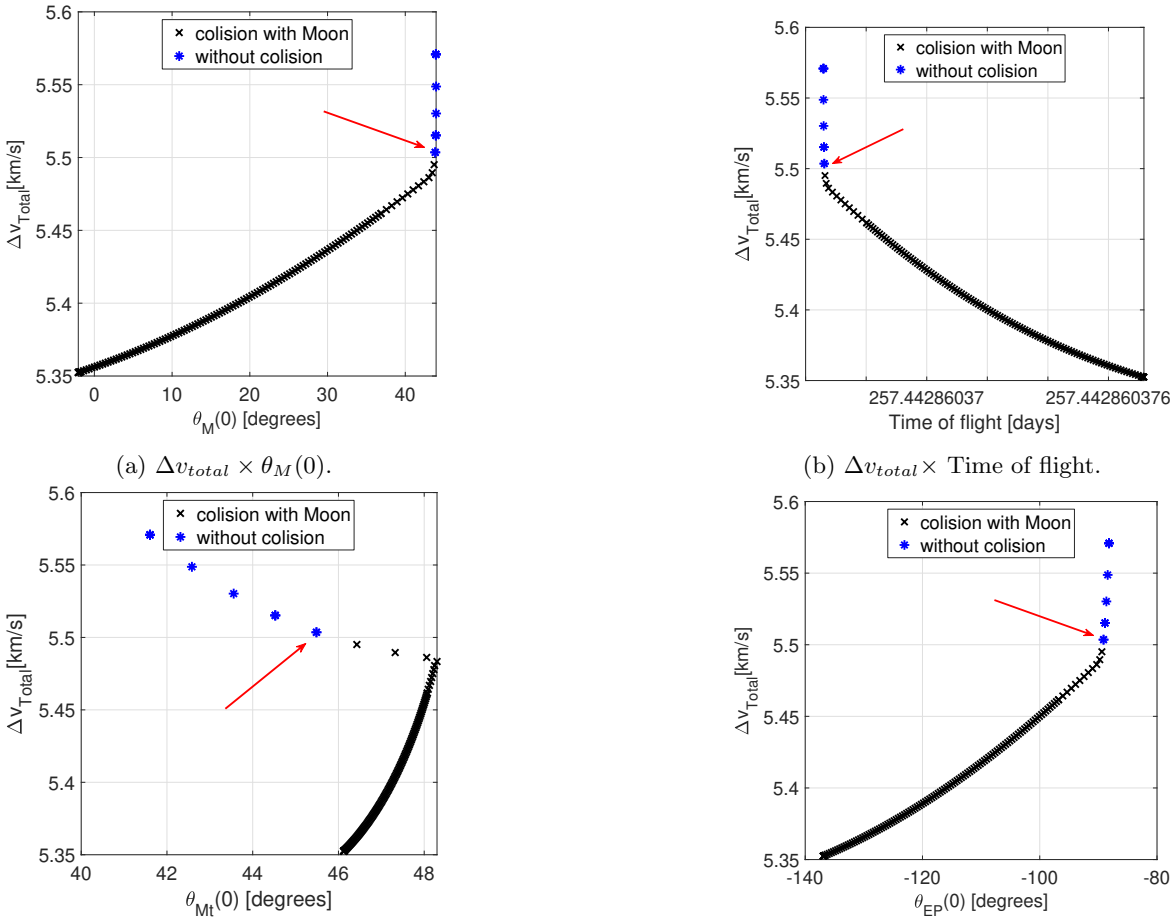

(a) $\Delta v_{total} \times \theta_M(0)$.

(b) $\Delta v_{total} \times$ Time of flight.

(c) $\Delta v_{total} \times \theta_{M_t}(0)$.

(d) $\Delta v_{total} \times \theta_{EP}(0)$.

Fig. 25. Earth-Mars mission with a lunar swing-by maneuver. The color figure can be viewed online.

to the Mars's SOI (Figure 26b) are practically the same, and both are close to the initial guess trajectory, which arrives closer to the tangent of the orbital motion of Mars. The complete view of the trajectories (Figure 26d) reveals that the local effect of the lunar swing-by maneuver does not have much influence on the complete trajectory, so, the time of flight of the three trajectories is basically the same.

For the Earth-Venus mission, the initial guess for the SGRA also does not collide with the Moon (Figure 27). The minimum fuel consumption solution is reached at 6.583586 km/s, i.e., a decrease of 307.201 m/s. The initial phase angle of the Moon decreases 13.016° (Figure 27a), the rendezvous angle increases 11.438° (Figure 27c), and the initial phase angle of the space vehicle decreases by about 15.191° (Figure 27d). The time of flight, similar to that of the Earth-Mars mission, almost does not change during the optimization algorithm, staying at 142.697 days (Figure 25b). Also, as trajectories with smaller fuel consumption are obtained by SGRA, the distance of the periselenium for the swing-by maneuver is smaller, so that the optimal solution collides with the Moon. For a practical purpose, the interesting solution is the one that does not collide with the Moon, which is indicated by the red arrow in Figure 27; results are highlighted in Table 11 in comparison to the solution based on the PCR4BP. Therefore, the design of a lunar swing-by maneuver for the Earth-Mars mission saves up to 170.913 m/s of fuel consumption without many changes in the time of flight, which increases by only 3.069 days, and without many changes in the rendezvous angle, which increases only 0.68° (Table 11). By observing Figures 27a, 27d, and Figure 27c the departure geometry must be accurate; otherwise, the space vehicle collides with the Moon. By considering a window for the rendezvous angle, Figure 27c, of only 11.464° in which there are trajectory solutions with a lunar swing-by maneuver without collision, a maxi-

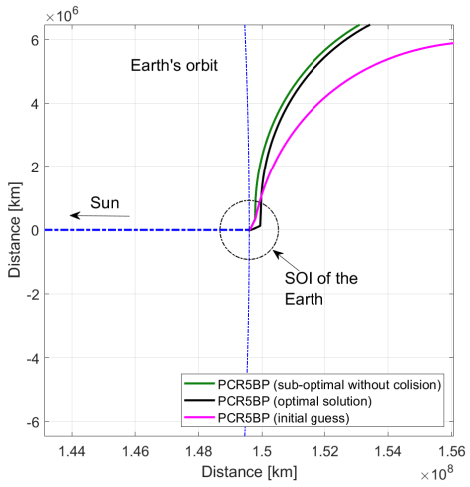

(a) Earth rotating reference frame centered at Sun.

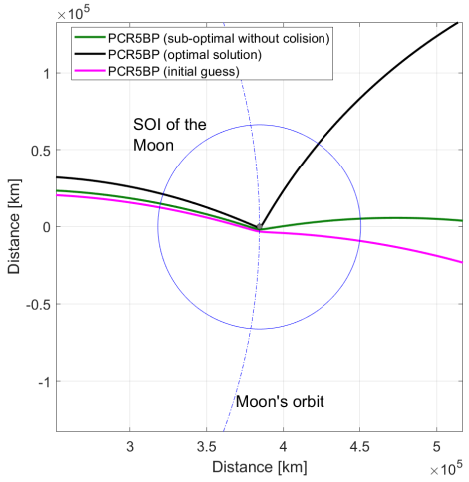

(b) Moon rotating reference frame centered at Earth.

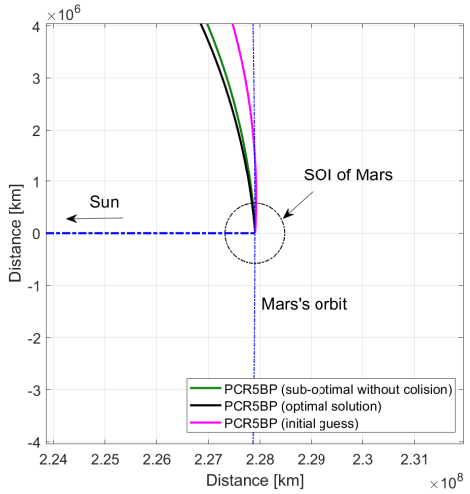

(c) Mars rotating reference frame centered at Sun.

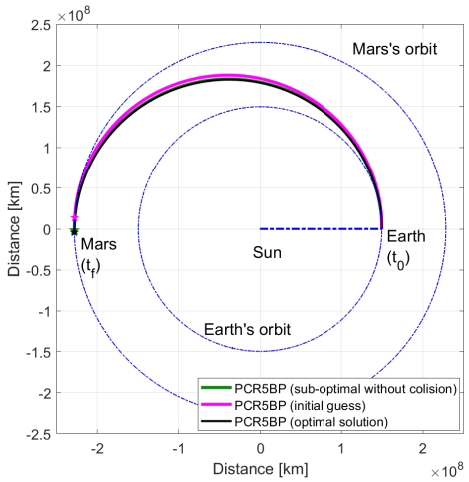

(d) Complete trajectory in the inertial reference frame centered at Sun.

Fig. 26. Optimal Earth-Mars trajectory with a lunar swing-by maneuver. The color figure can be viewed online.

mum penalty on the fuel consumption of 275.285 m/s is observed. Similar to the Earth-Mars mission, the results of the trajectory without collision with the Moon for the Earth-Venus mission is, actually, a sub-optimal result extracted from the convergence of the optimization algorithm, so, it depends on the trajectory that initializes this algorithm.

Figure 28 plots three Earth-Venus trajectories with lunar swing-by maneuver: the first one is used as the initial solution to initialize the SGRA (magenta color); the second one is the optimal solution determined by the SGRA (black color), the third one is the smaller fuel consumption trajectory without collision with the Moon, also determined by the SGRA (green color). Note in Figures 28a and 28b the huge deflection of the black trajectory. As the SGRA computes smaller fuel consumption trajectories, the distance of the periselenium on the swing-by maneuver decreases until the optimal trajectory is reached (black color). For the smaller fuel consumption trajectory without collision with the Moon, the altitude of the periselenium is just 44.468 km. In order to prescribe the periselenium altitude, one can add an intermediary constraint for the altitude of the swing-by maneuver; however, this problem becomes harder to solve since it becomes more restrictive. An interesting comparison between the Earth-Mars and the Earth-Venus mission is observed in Figures 26a and 28a: for the Earth-Mars mission, the lunar swing-by maneuver occurs when the Moon is ahead the Earth and farther from the Sun than Earth (Figure 26a); on the other hand,

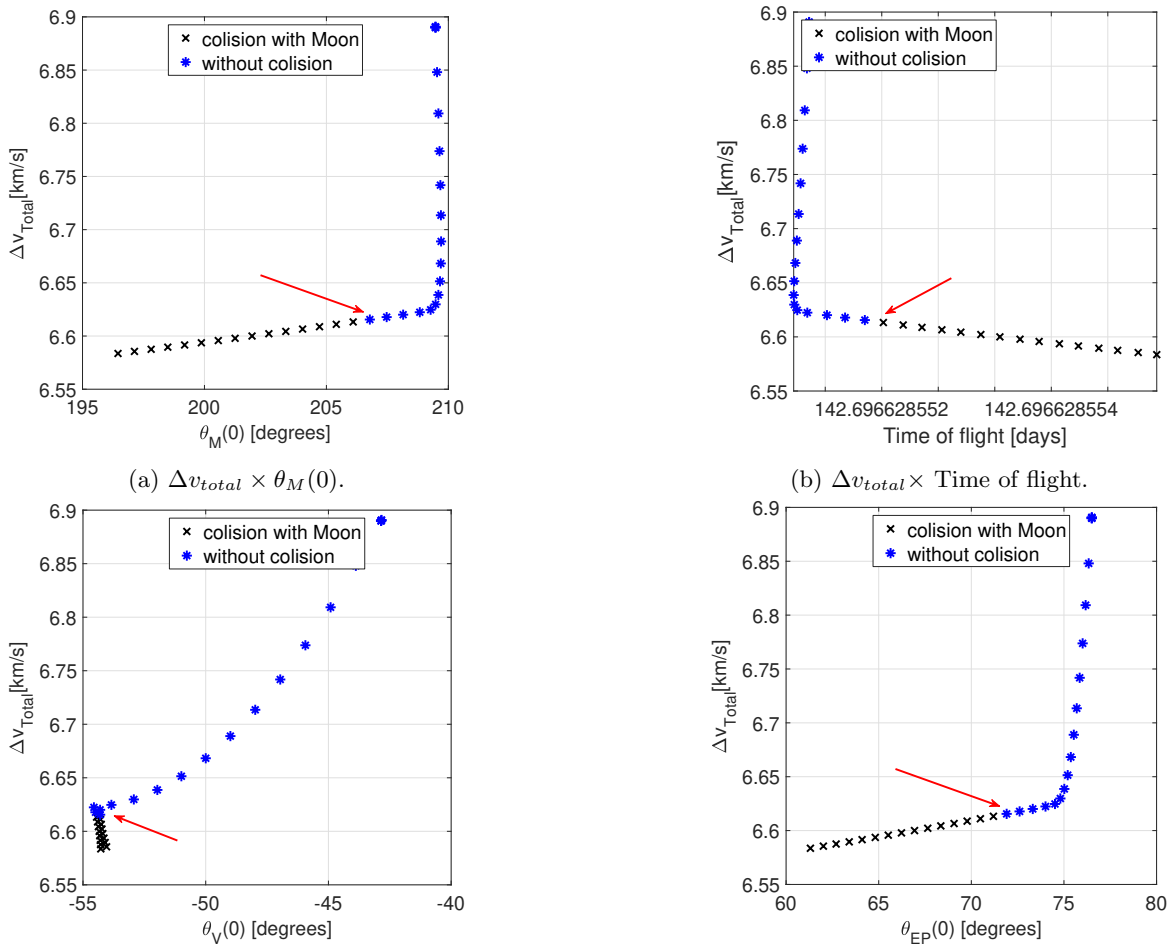

(a) $\Delta v_{total} \times \theta_M(0)$.

(b) $\Delta v_{total} \times$ Time of flight.

(c) $\Delta v_{total} \times \theta_V(0)$.

(d) $\Delta v_{total} \times \theta_{EP}(0)$.

Fig. 27. Earth-Venus mission with a lunar swing-by maneuver. The color figure can be viewed online.

TABLE 11

MAIN PARAMETERS FOR THE SMALLEST FUEL CONSUMPTION TRAJECTORIES FOR EARTH-VENUS MISSION WITH AND WITHOUT A LUNAR SWING-BY MANEUVER

Model	Δv_{LEO} [km/s]	Δv_{LM_tO} [km/s]	Δv_{Total} [km/s]	Time of Flight [days]	$\theta_V(T)$ [degrees]	$\theta_{EP}(0)$ [degrees]	$\theta_V(0)$ [degrees]
PCR4BP[1]	3.449138	3.337284	6.786422	139.628	173.795	105.084	-50.060
PCR5BP[2]	3.275623	3.339886	6.615509	142.697	174.475	71.907	-54.300

[1]Results from the two degree-of-freedom optimization problem based on the PCR4BP.

[2]Results from the two degree-of-freedom optimization problem based on the PCR5BP without a collision with the Moon.

for the Earth-Venus mission, the lunar swing-by maneuver occurs when the Moon is behind the Earth and closer to the Sun than Earth. In both cases, however, the swing-by maneuver occurs in a counterclockwise sense, since the space vehicle must accelerate during the swing-by maneuver. These differences in the position of the Moon are related to the type of transfer: inner transfer or outer transfer. For the outer transfer (Earth-Mars mission), the space vehicle must leave the SOI of Earth from ahead according to the Hohmann transfer; and, for the inner transfer (Earth-Venus mission), the space vehicle must leave

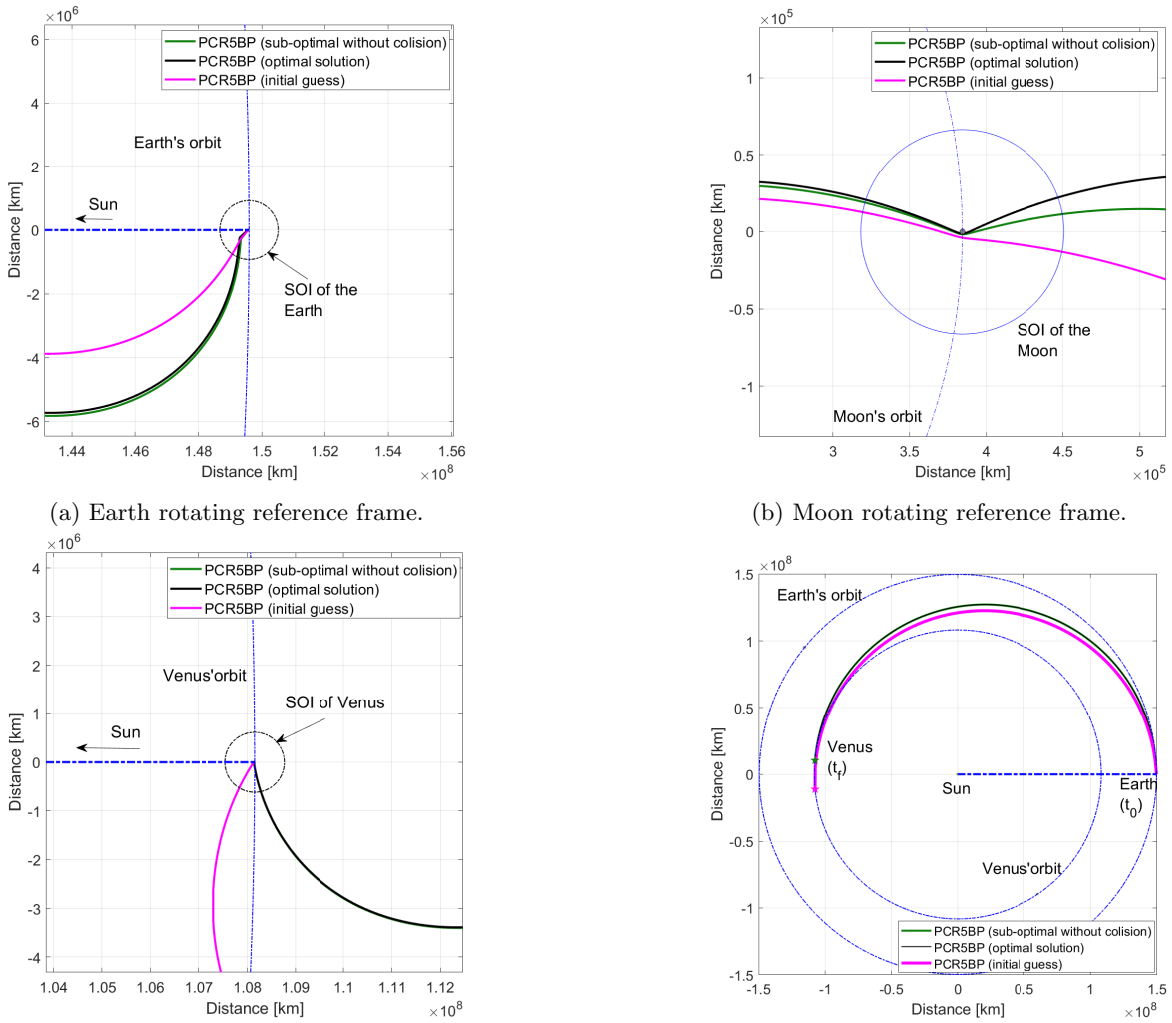

(a) Earth rotating reference frame.

(b) Moon rotating reference frame.

(c) Venus rotating reference frame.

(d) Complete trajectory in the inertial reference frame centered at Sun.

Fig. 28. Optimal Earth-Venus trajectory with a lunar swing-by maneuver. The color figure can be viewed online.

the SOI of Earth from behind. Therefore, the lunar swing-by maneuver aids the space vehicle to achieve the hyperbolic excess velocity, which corresponds to an accelerative velocity increment of the Hohmann transfer for an outer mission, or it corresponds to a decelerating velocity increment of the Hohmann transfer for an inner mission.

Tables 12 and 13 compile the results already seen with the best transfer with and without lunar swing-by maneuver. The results determined by Miele and Wang (1999b) for the Earth-Mars mission are also repeated in order to highlight the similarity of the results determined by Miele and Wang (1999b) and the ones calculated in this work, specifically in the context of the PCR4BP. A detailed discussion about this result was already done in § 3.1 and § 3.2. As a final remark, Prado (2003) calculates the saving of fuel consumption due to a lunar swing-by maneuver for interplanetary trajectories based on the Hohmann transfer. In this way, for an altitude of the lunar swing-by maneuver of 102 km, Prado (2003) determines a saving of 124 m/s for the Earth-Mars mission, and a saving of 137 m/s for the Earth-Venus mission. For an altitude of the lunar swing-by maneuver of 12 km, Prado (2003) determines a saving of 129 m/s for the Earth-Mars mission, and a saving of 142 m/s for the Earth-Venus mission. The savings of fuel consumption for a more high fidelity model as the PCR5BP determined by the present work are practically the same as those determined by Prado (2003) or even a little larger: for the Earth-Mars mission the saving reaches 148

TABLE 12

MAIN PARAMETERS FOR THE SMALLEST FUEL CONSUMPTION TRAJECTORIES FOR EARTH-MARS MISSION

Model	Δv_{LEO} (km/s)	Δv_{LM_tO} (km/s)	Δv_{Total} (km/s)	Time of Flight (days)
PCR4BP[1]	3.551905	2.100124	5.652029	257.861
Miele[2]	3.552000	2.100000	5.652000	257.880
Patched-conic based on Hohmann	3.555746	2.101260	5.657006	264.430
Patched-conic based on Gauss	3.555572	2.101454	5.657026	263.579
Patched-conic detailed geometry[3]	3.514668	2.087434	5.602101	257.965
Patched-conic lunar swing-by PCR5BP[4]	3.362211	2.086891	5.449101	257.443
Lunar swing-by	3.404922	2.098633	5.503555	257.443

[1]Results from a two degree-of-freedom optimization problem.

[2]Results based on the PR4CP calculated by Miele and Wang (1999b).

[3]Smallest fuel consumption trajectory found for $\lambda_{Mt} = 89^\circ$ (arrival ahead the SOI).

[4]Results from the two degree-of-freedom optimization problem based on the PCR5BP without a collision with the Moon.

TABLE 13

MAIN PARAMETERS FOR THE SMALLEST FUEL CONSUMPTION TRAJECTORIES FOR EARTH-VENUS MISSION

Model	Δv_{LEO} (km/s)	Δv_{LVO} (km/s)	Δv_{Total} (km/s)	Time of Flight (days)
PCR4BP[1]	3.449138	3.337284	6.786422	139.628
Patched-conic based on Hohmann	3.447245	3.339810	6.787055	151.822
Patched-conic based on Gauss	3.447417	3.339550	6.786967	151.771
Patched-conic detailed geometry [2]	3.406312	3.294024	6.700336	147.976
Patched-conic lunar swing-by PCR5BP[3]	3.376566	3.289849	6.666415	149.440
Lunar swing-by	3.275623	3.339886	6.615509	142.697

[1]Results from a two degree-of-freedom optimization problem.

[2]Smallest fuel consumption trajectory found for $\lambda_V = -87^\circ$ (arrival behind the SOI).

[3]Results from the two degree-of-freedom optimization problem based on the PCR5BP without a collision with the Moon.

m/s (compare Δv_{Total} between the PCR4BP and the PCR5BP in Table 12). In this case, the altitude of the lunar swing-by maneuver is 78.313 km, which is larger than the 12 km altitude specified by Prado (2003). For the Earth-Venus mission the saving reaches 137 m/s (compare Δv_{Total} between the PCR4BP and the PCR5BP in Table 13). In this case, the altitude of the lunar swing-by maneuver,

44.468 km, is also larger than the 12 km altitude specified by Prado (2003). Therefore, despite the calculated savings being similar in the present work to the ones of Prado (2003), the higher fidelity model, based on the PCR5BP, provides trajectories with a larger lunar swing-by altitude for both missions, which increase the operational feasibility of the mission.

4. CONCLUSION

This work describes two-point boundary value problems to determine interplanetary trajectories with and without lunar swing-by maneuvers considering several models: patched-conic approximation based on Hohmann transfer, patched-conic approximation based on the Gauss problem; patched-approximation associated with a boundary problem; patched-conic approximation associated with a boundary problem and with an intermediary constraint that defines a lunar swing-by maneuver; a model based on the four-body problem; and a model based on the five-body problem. The comparison of the models illustrates that the patched-conic approximations provide good initial guesses for more complex models such as the PCR4BP and the PCR5BP models, making the convergence of the optimization problems easier.

The first part of the present work analyses interplanetary missions without a lunar swing-by maneuver. The interplanetary patched-conic with detailed geometry shows that the direction of the target orbit does not change the velocity increments, the time of flight, the rendezvous angle, and the initial phase angles of the space vehicle. The only difference due to the direction of the target orbit is the phase angle of the space vehicle at the arrival at the target orbit. Optimal interplanetary trajectories are computed in the context of the PCR4BP by a two-degree optimization problem. An analysis around the solutions of this two-degree optimization problem is performed by an one-degree optimization problem, which reveals that the penalty on the fuel consumption due to the delayed or early departures is more severe for the Earth-Venus mission than for the Earth-Mars mission. Future work can be accomplished to generalize and classify the results of the fuel consumption between interior and exterior planet missions.

The second part analyses interplanetary missions with a lunar swing-by maneuver. A first comparison is made between the results of a patched-conic approximation and the results of a model based on the PCR5BP, and it shows the possibility to save fuel consumption without changing the time of flight. These first solutions are utilized to initialize a three-degree of freedom optimization problem in which the position of the Moon, the rendezvous angle, the velocity increments, the time of flight, and the initial phase angle of the space vehicle are set as unknowns to minimize the fuel consumption. The results show that the optimal trajectory for the Earth-Mars and Earth-Venus mission collides with the Moon during the swing-by maneuver. However, sub optimal solutions that do not collide with the Moon are practical presenting a significant saving of fuel consumption without many changes on the time of flight when they are compared to the solutions without a lunar swing-by maneuver.

This research is supported by grant 2012/25308-5, São Paulo Research Foundation (FAPESP), and by CNPq under contract 301875/2017-0.

REFERENCES

Abdelkhalik, O. & Mortari, D. 2007, JSpRo, 44, 456, https://doi.org/10.2514/1.24701

Addis, B., Cassioli, A., Locatelli, M., & Schoen, F. 2011, Computational Optimization and Applications, 48, 635, https://doi.org/10.1007/s10589-009-9261-6

Batte, R. R., Mueller, D. D., & White, J. E. 1971, Fundamentals of astrodynamics (New York, NY: Dover Publications)

Battin, R. H. & Vaughan, R. M. 1984, JGCD, 7, 662, https://doi.org/10.2514/3.19910

Battin, R. H., Fill, T. J., & Shepperd, S. W. 1978, JGCD, 1, 50, https://doi.org/10.2514/3.21004

Bayer, T., Buffington, B., Castet, J.-F., et al. 2017, Europa mission update: Beyond payload selection, IEEE Aerospace Conference Proceedings, https://doi.org/10.1109/AERO.2017.7943832

Broucke, R. A. 1988, The celestial mechanics of gravity assist, AIAA/AAS Astrodynamics Conference (Washington, DC: AIAA), 69

Cichan, T., Bailey, S. A., Norris, S. D., et al. 2017, Mars Base Camp: An Architecture for Sending Human to Mars, IEEE Aerospace Conference

Daukantas, P. 2017, OptPN, 28, 26, https://doi.org/10.1364/OPN.28.5.000026

Dei Tos, D. A. & Topputo, F. 2019, JGCD, 42, 1343, https://doi.org/10.2514/1.g003838

Ellison, D. H., Conway, B. A., Englander, J. A., & Ozimek, M. T. 2018, JGCD, 41, 1149, https://doi.org/10.2514/1.g003077

Faria Venditti, F. C., Marconi Rocco, E., Bertachini De Almeida Prado, A. F., & Suhkanov, A. 2010, AcAau, 67, 1255, https://doi.org/10.1016/j.actaastro.2010.06.022

Foust, J. 2019, Gateway or bust: NASA's plan for a 2024 lunar landing depends on a much-criticized orbital outpost, IEEE Spectrum, 56, 32, https://doi.org/10.1109/mspec.2019.8747310

Gagg Filho, L. A. & da Silva Fernandes, S. 2016, Computational and Applied Mathematics, 35, 753, https://doi.org/10.1007/s40314-015-0247-y

_____. 2018, Computational and Applied Mathematics, 37, 27, https://doi.org/10.1007/s40314-017-0529-7

Genta, G. & Maffione, F. 2019, Choice of the Optimal Launch Date for Interplanetary Missions in Springer Optimization and Its Applications, ed. G. Fasano & J. Pintér, 111, https://doi.org/10.1007/s40314-017-0529-7

Gooding, R. H. 1990, CEMDA, 48, 145, https://doi.org/10.1007/BF00049511

Izzo, D., Sprague, Ch. I., & Tailor, D. V. 2019, Machine Learning and Evolutionary Techniques in Interplanetary Trajectory Design in Springer Optimization and Its Applications, ed. G. Fasanu & D. Pintér, 191, https://doi.org/10.1007/978-3-030-10501-3_8

Lavagna, M., Povoleri, A., & Finzi, A. E. 2005, AcAau, 57, 498, https://doi.org/10.1016/j.actaastro.2005.03.052

Lorenz, R. D., Turtle, E. P., Barnes, J. W., et al. 2018, JHATD, 34, 374

Marec, J. P. 1979, Optimal space trajectories (Amsterdam, Netherlands: Elsevier Scientific Publishing)

Meiss, J. H., Jaeger, M., Gronowski, M., Kachler, T., & Dickens, K. 2016, Evolution and Status of the Orion-ESM Propulsion Subsystem, AIAA, https://doi.org/10.2514/6.2016-5622

Miele, A. & Wang, T. 1997, JOTA, 95, 467, https://doi.org/10.1023/A:1022661519758

_____. 1999a, AcAau, 45, 655, https://doi.org/10.1016/s0094-5765(99)00117-4

_____. 1999b, AcAau, 45, 119, https://doi.org/10.1016/S0094-5765(99)00109-5

Miele, A., Huang, H. Y., & Heideman, J. C. 1969, JOTA, 4, 213, https://doi.org/10.1007/BF00927947

Miele, A., Wang, T., & Mancuso, S. 2004a, AcAau, 55, 79, https://doi.org/10.1016/j.actaastro.2003.12.018

Miele, A., Wang, T., & Williams, P. N. 2004b, AcAau, 55, 95, https://doi.org/10.1016/j.actaastro.2004.01.053

O'Dell, S. & Cichan, T. 2018, Crewed Missions to the Martian Surface via Mars Base Camp, AIAA 2018 SPACE and Astronautics Forum and Exposition, https://doi.org/10.2514/6.2018-5142

Petrescu, R. V., Aversa, R. A., Akash, B., et al. 2017, Lockheed Martin-A Short Review in Journal of Aircraft and Spacecraft Technology, 1, 50, https://doi.org/10.3844/jastsp.2017.50.68

Prado, A. F. B. A. 2003, J. Braz. Soc. Mech. Sci. & Eng., 25, https://doi.org/10.1590/S1678-58782003000200003

Press, W. H., Teukolsky, S. A., Vetterling, W. T., & Flannery, B. P. 1997, Numerical Recipes in Fortran 77. The Art of Scientific Computing

Prussing, J. E. 1979, JGCD, 2, 442, https://doi.org/10.2514/3.55905

Prussing, J. E. & Chiu, J. H. 1986, JGCD, 9, 17, https://doi.org/10.2514/3.20060

Prussing, J. E. & Conway, A. 1993, Orbital Mechanics, OUP, 1993

Shepard, M. K., Richardson, J., Taylor, P. A., et al. 2016, Icar, 281, 388, https://doi.org/10.1016/j.icarus.2016.08.011

Tsuda, Y., Yoshikawa, M., Saiki, T., Nakazawa, S., & Watanabe, S. 2018, AcAau, 156, 387, https://doi.org/10.1016/j.actaastro.2018.01.030

Weinzierl, M. 2018, Journal of Economic Perspectives, 32, 173, https://doi.org/10.1257/jep.32.2.173

Yang, B., Yang, H., & Li, S. 2019, AcAau, 165, 139, https://doi.org/10.1016/j.actaastro.2019.09.006

Sandro da Silva Fernandes: Mathematics Department, Instituto Tecnológico de Aeronáutica, Praça Marechal Eduardo Gomes 50, Vila das Acácias, 12228-900, São José dos Campos, SP, Brazil (sandro@ita.br).

Luiz Arthur Gagg Filho: Flight Mechanics Department, Instituto Tecnológico de Aeronáutica, Praça Marechal Eduardo Gomes 50, Vila das Acácias, 12228-900, São José dos Campos, SP, Brazil (arthurga@ita.br).